Targeting Troponin I Phosphorylation for Precision Treatment of Diastolic Dysfunction

Ying-Chi Chao[1], Debra J. McAndrew[3#], David Revuelta[2], Rahul Yadav[1], Wan-Hua Hong[1], Jianshu Hu[1], Milda Folkmanaite[1], Edoardo Valli[1], Mariana Gee Olmedilla[1], Andreas Koschinski[1], Nicoletta C. Surdo[1°], Jakub Tomek[1], Helen Edwards[4], Connor Blair[4], Evaldas Girdauskas[5], David Henderson[4], Josh Hurst[6], Adam Linekar[6], Yiangos Psaras[3], Julia Gorelik[7], Nicola Smart[1], Christopher Toepfer[3], Helen Maddock[6,8], George Baillie[4], Craig A. Lygate[3,4], Cristina E. Molina[1,2], Manuela Zaccolo[1*]

[1]Department of Physiology Anatomy and Genetics, University of Oxford, UK; [2]Institute of Experimental Cardiovascular Research, University Medical Center Hamburg-Eppendorf, Germany; [3]Radcliffe Department of Medicine, University of Oxford, UK; [4]College of Veterinary, Medical and Life Sciences, University of Glasgow, UK; [5]Department of Cardiovascular Surgery, University Heart Center Hamburg, Germany; [6]Coventry University Group, Coventry University, UK; [7]Imperial College, London, UK; [8]InoCardia Ltd, Coventry, UK.

[#]Current address: Target Discovery Institute, University of Oxford; °current address: Neuroscience Institute, National Research Council of Italy (CNR) and Veneto Institute of Molecular Medicine, Foundation for Advanced Biomedical Research, Padova, Italy.

*Correspondence to:

Manuela Zaccolo
Department of Physiology Anatomy and Genetics
University of Oxford
Sherrington Building
Parks Road
OX1 3PT Oxford, UK
manuela.zaccolo@dpag.ox.ac.uk

Abstract

Background: Defective cardiac relaxation (diastolic dysfunction) is prevalent in heart failure, particularly in the context of diabetes, obesity, hypertension, and ageing, and is associated with increased mortality. Yet no effective therapy directly targets this abnormal relaxation. Phosphorylation of troponin I by cAMP-dependent protein kinase A (PKA) promotes relaxation, but global PKA activation has widespread, undesirable effects. Here we investigated whether selectively enhancing troponin I phosphorylation could improve relaxation without engaging the broader PKA signalling network.

Methods: To resolve cAMP signalling at subcellular scales, we combined real-time cAMP measurements with FRET-based genetically encoded reporters targeted to defined nanodomains, alongside biochemical and genetic approaches. Protein–protein interaction surfaces were mapped using peptide-array technology, which guided the design of a disruptor peptide to displace specific interactions. The peptide's effects on cardiomyocyte function were assessed *in vitro* using rodent and human cardiomyocytes with biochemical assays, real-time imaging, and work-loop analysis. *In vivo* effects were evaluated through echocardiography and haemodynamic measurements.

Results: We identified a previously unrecognized regulatory mechanism in which the cAMP-hydrolyzing enzyme PDE4D9 interacts with troponin I and restricts local cAMP levels within a nanometre-scale domain, thereby selectively controlling troponin I phosphorylation. We found that PDE4D9–troponin I association is markedly increased in cardiac disease in both rodents and humans. A peptide that displaces PDE4D9 from troponin I selectively enhances troponin I phosphorylation, accelerates cardiomyocyte relaxation, and prevents diastolic dysfunction in a mouse model of heart failure.

Conclusions: These findings reveal a highly specific regulatory nanodomain governing troponin I phosphorylation and points to a first-in-class, mechanism-based therapeutic strategy with the potential to address a major unmet contributor to heart failure.

Clinical Perspective

What Is New?

- We identify a previously unrecognized, nanometre-scale regulatory mechanism in which PDE4D9 binds troponin I to locally suppress cAMP and limit troponin I phosphorylation.
- We demonstrates that the PDE4D9–troponin I interaction is markedly upregulated in failing hearts in both rodents and humans, which can mechanistically explain the impaired cardiac relaxation.
- We show that this interaction is druggable: a rationally designed peptide can selectively displace PDE4D9, restore localized cAMP–PKA signalling, and normalize myocardial relaxation without global cAMP perturbation.

What Are the Clinical Implications?

- Diastolic dysfunction, a major cause of heart failure with no targeted treatments, may be amenable to therapies that modulate cAMP signalling with subcellular precision rather than global pathway modulation.
- Selective disruption of PDE4D9–troponin I binding offers a mechanism-based approach with potential to restore diastolic function while minimizing off-target effects typical of GPCR-directed therapies.
- More broadly, this work establishes a platform for targeting localized signalling domains, a concept that may extend beyond cardiovascular disease to other pathological conditions in which dysregulated cAMP contributes to dysfunction.

Introduction

Cardiac contraction (systole) and relaxation (diastole) are driven by contractile proteins arranged in sarcomeres consisting of interdigitated thick myosin and thin actin filaments (Fig. 1b). The sliding of thick and thin filaments past each other causes the sarcomeres to shorten during contraction and re-lengthen during relaxation. This process is regulated by the binding and unbinding of Calcium ions to and from troponin C (TPNC) which, together with troponin T (TPNT) and troponin I (TPNI), forms the regulatory troponin complex associated with the thin filament. During sympathetic stimulation, activation of the β-adrenergic receptor (β-AR)/cAMP/ PKA pathway leads to phosphorylation of multiple targets, including proteins that enhance contraction and relaxation, allowing the heart to adapt to higher workload demands. PKA phosphorylation of phospholamban (PLB) at the sarcoplasmic reticulum (SR) enhances the activity of the sarco-endoplasmic reticulum Calcium ATPase (SERCA), promoting Calcium reuptake into the SR and ensuring a greater Calcium reserve is available for release during the next contraction. PKA phosphorylation of the thick filament protein myosin-binding protein C (MyBPC) enhances contraction by extending the force-generating state of the sarcomere. Phosphorylation of TPNI facilitates relaxation by lowering the affinity of TPNC for Calcium, ensuring timely deactivation of myofilaments to match faster contraction rate[1]. In pathological conditions, such as heart failure (HF), chronic β-AR overstimulation disrupts cAMP signaling, impairing contractility and relaxation[2]. β-blockers mitigate these effects and improve cardiac efficiency by reducing oxygen demand and preventing further myocardial damage[3]. However, β-blockers are ineffective when the primary issue is not impaired contraction but inadequate cardiac relaxation[4].

The cAMP/PKA signalling pathway operates through a complex network of subcellular signalling nanodomains[5]. Elevation of cAMP following G-protein–coupled receptor (GPCR) activation is not uniformly distributed within cardiomyocytes. Instead, receptor-specific, nanometer-scale cAMP gradients are established across the cell, governed by the localized activity of cAMP-hydrolyzing phosphodiesterases (PDEs)[6]. The spatially confined cAMP nanodomains activate a selected subset of PKA enzymes, typically tethered in proximity of specific phosphorylation targets via scaffolding proteins named A-kinase anchoring proteins (AKAPs)[7]. This spatial

organization allows selective phosphorylation of local targets, resulting in cellular effects that exhibit a distinct profile, ensuring signalling specificity[8]. While drugs targeting the GPCR influence the entire intracellular network of the receptor-associated cAMP nanodomains and the full spectrum of its functional effects, the compartmentalized nature of cAMP signalling offers the opportunity for a more precise intervention[9]. Such an approach could selectively modulate cAMP levels within an individual compartment achieving nanometer subcellular precision and stringent functional selectivity[5].

We previously demonstrated that the cAMP signal generated upon β-AR activation at TPNI is distinctly regulated compared to the cAMP signals that the same stimulus generates at the plasmalemma or the SR[6]. This observation prompted us to investigate whether TPNI defines a distinct cAMP nanodomain that could be selectively targeted to enhance relaxation for the treatment of diastolic dysfunction.

Methods:

Materials & Reagents

Isoproterenol, cilostamide, rolipram, forskolin, and 3-isobutyl-1-methylxanthine (IBMX) were from Sigma-Aldrich; N-terminal stearic-scrambled peptide (SC, KTELKAERGIKSDVAKERELHDLGK) and disrupting peptide (P33, GTRAKESLDLRAHLKQVKKEDIEKE) were synthesised by GenScript. Collagenase A was from Roche; pancreatin was from Sigma; laminin (mouse) was from BD Biosciences; PBS, DMEM high glucose, MEM199, horse serum, newborn calf serum (NCS), penicillin/streptomycin (10,000 units/ml of penicillin and 10,000 μg/ml of streptomycin), and L-glutamine were from

Invitrogen. Adenoviral vectors and self-complementary AAV vectors carrying the target reporter and sequences were generated by Vector Biolabs (Malvern, PA, USA).

Generation of MyBPC-CUTie targeted reporter

Full length mouse cardiac myosin binding protein C (MyBPC, NM_008653.2) was PCR-amplified to incorporate NheI restriction sites at both 5’ and 3’ ends. The resulting fragment was cloned, in frame, into the NheI site of the CUTie sensor[6]. Clones were screened for correct orientation of insert and selected clones were sequenced.

Adenoviral vector carrying the MyBPC-CUTie targeted reporter was generated by Vector Biolabs (Malvern, PA, USA)

Primary cardiac myocyte isolation

ARVMs were isolated from 300-350 g male Sprague Dawley rats as described[10]. Briefly, hearts were perfused on a Langendorff apparatus at 37 °C for 4-5 min through the coronary arteries with an oxygenated Calcium-free Tyrode Buffer solution (130 mM NaCl, 5 mM Hepes, 0.4 mM NaH_2PO_4, 5.6 mM KCl, 3.5 mM $MgCl_2$, 20 mM Taurine, 10mM Glucose), and subsequently digested with 0.06 mg/ml Liberase TH (Roche Diagnostics Limited, UK) in a 10 μM Calcium Tyrode Buffer solution with addition of 10 μM Blebbistain (T6038, TargetMol Chemicals, USA) for a further 15-20 min until the heart became flaccid. After perfusion, the left ventricle was removed, minced, and resuspended in equal volume of 1% BSA Calcium-free Tyrode Buffer solution. Extracellular Calcium was added incrementally to reach a final concentration of 1.0 mM. Cells were cultured in Minimum Essential Medium (MEM) (Sigma-Aldrich, UK), supplemented with 2.5% foetal bovine serum (FBS), 1% penicillin-streptomycin, 1% L-Glutamine and 9 mM $NaHCO_3$ and plated on laminin (40 μg/ml) coated culture dishes. ARVMs were left to adhere for 2 h in a 5% CO_2 atmosphere at 37 °C, before the medium was replaced with FBS-free MEM. Myocytes were infected for 3 h at multiplicity of infection (MOI) of 10–100 with adenovirus encoding for FRET reporters. The medium was then replaced with fresh FBS-free MEM including 0.5 μM cytochalasin D (MP Biomedicals, UK). Infected cells were kept in culture for less than 36 h. NRVM were cultured as described before[11].

Immunostaining

ARVMs plated on coverslips were infected for 2 h at a MOI of 10-100 with adenovirus encoding for CUTie sensors. After 48 h of infection, cell were washed 3x with PBS, and fixed with 4% PFA in PBS at room temperature for 15 min. After permeabilisation with PBS+0.2% Triton-X-100 (PBST) for 30 min, the coverslips were blocked in PBST+1% BSA for 1 h at room temperature. Primary α-Actinin antibody (Abcam, ab9465, 1:400) incubation was performed overnight at 4°C, followed by 3 washes at room temperature with PBS+0.025% Tween 20 and incubation with an Alexa Fluor 647 (Invitrogen, A-21235, 1:500) conjugated secondary antibody

for 1 hour. Coverslips were mounted in Ibidi mounting medium (Thistle Scientific). Confocal images were acquired using a Leica Stellaris TauSTED Xstend microscope (Leica, Wetzlar, Germany), and the images were analysed using Leica LAS X software (Leica, Wetzlar, Germany).

Primary cardiomyocytes siRNA knockdown

Silencer pre-designed PDE4B siRNA (Assay ID: 200641), PDE4D siRNA (Assay ID: 200644), and Silencer negative control No.1 siRNA (AM4611) were purchased from Thermo Fisher Scientific. $2x10^6$ NRVM were plated onto 6-well plate coated with laminin (0.75 µg/cm^2). One day after plating the medium was replaced with low-serum (0.5% NCS) DMEM medium. Individual siRNA with indicated concentrations were transfected into NRVM using Lipofectamine RNAiMax transfection reagent (133778030, Thermo Fisher Scientific) following the manufacture's protocol. 48 h after transfection, the cells were harvested for Western blots or FRET experiments.

FRET imaging

FRET imaging experiments were performed 24-48 h after transduction with adenovirus carrying each sensor, as previously described[12]. For the measurements, cells were maintained at room temperature in a modified Ringer solution (125 mM NaCl, 20 mM Hepes, 1 mM Na_3PO_4, 5 mM KCl, 1 mM $MgSO_4$, 5.5 mM Glucose, $CaCl_2$ 1mM, pH 7.4). ARVMs were imaged 18 h after infection and kept at ~35 °C in a modified Tyrode solution containing 1.4 mM Calcium. An inverted microscope (Olympus IX71) with a PlanApoN, 60X, NA 1.42 oil immersion objective, 0.17/FN 26.5 (Olympus, UK), was used for image acquisition. The microscope was equipped with a CoolSNAP HQ2 monochrome camera (Photometrics) and a DV2™ optical beam-splitter (MAG Biosystems, Photometrics). Images were acquired and processed using MetaFluor® 7.1, (Meta imaging series, Molecular Devices). FRET changes were measured as changes in the background-subtracted 480nm/535nm fluorescence emission intensity on excitation at 430 nm and expressed as R/R_0, where R is the ratio at time t and R_0 is the average ratio of the first 8 frames.

Immunoprecipitation

For pull-down experiments, ARVM isolated from one heart were suspended in Tyrode buffer with 1.4 µM Calcium and treated as described. For NRVM pull-down, $6x10^6$ NRVM were plated onto 10-cm Petri dishes coated with laminin (0.2 µg/cm^2) and infected with the indicated adenovirus for 36-48 hours and treated as

described. For hiPSC-CMs pull-down, $1x10^6$ hiPSC-CMs were plated to 6-cm Petri dishes 30 days after differentiation and treated as describe. For heart tissue, freshly isolated ventricles (≈50–100 mg) were homogenized on ice, while cultured cells were harvested directly in ice-cold IP buffer (50 mM HEPES pH7.4, 150 mM NaCl, 2 mM EDTA, 10% glycerol, 0.5% Triton-X-100 or 50 mM Tris pH7.4, 150 mM NaCl, 1 mM EDTA, 10% glycerol, and 1% nonyl phenoxypolyethoxylethanol [NP40]) supplemented with Complete EDTA-free protease inhibitor cocktail tablets and a 'PhosSTOP' Phosphatase Inhibitor Cocktail Tablet (Roche Diagnostics Limited) for 5min on ice. The cells were then collected and placed on a rotating wheel for 20 min at 4^oC. Insoluble material was removed by centrifugation at 17,000g for 10 min at 4° C and total protein was quantified by Micro BCA Protein Assay Kit (Pierce Biotechnology Inc.). 500-1000 μg proteins were rotated for 1 h at 4^oC with 20 μl Pierce protein A Plus agarose (Thermo Fisher Scientific, 22810). The precipitates were removed by centrifugation at 1,000g for 3 min. Supernatants were then rotated overnight with a monoclonal anti-cardiac troponin I (Abcam, ab10231, 1:250), followed by 30 μl protein G agarose beads (Cell signalling, 37478) for 2-4 h. The precipitates were than collected by centrifugation at 1,000g for 3 mins and beads were washed three times with ice-cold IP buffer. Bound proteins were then eluted in 60 μl of 2X SDS loading buffer (Life Technologies) and released from the beads at 96^oC for 6 min.

Western blotting

Pull-down proteins and samples equivalent to 20-50 μg proteins were separated on NuPage 4-12% Bis-Tris gradient gel (Invitrogen) and transferred onto PVDF blotting membrane (Amersham Hybond P 0.45 PVDF, Cytiva). After transfer, the membrane was blocked for 1 h at room temperature with 5% skim milk (VWR Chemicals) or 5% PhosphoBLOCKER blocking reagent (Cell Biolabs), and then incubated overnight at 4^oC with the following primary antibodies: mouse-anti-cardiac TPNI (Abcam, ab10231, 1:2000), rabbit anti-Phospho TPNI (S22+23) (Abcam, ab190697, 1:2000), mouse anti-PLN (Badrilla, A010-14, 1:4000), rabbit anti-phospho PLN (pSer16) (Badrilla, A010-12AP, 1:4000), mouse anti-MyBPC (Santa Cruz, sc-137237, 1:500), rabbit anti-phospho MyBPC (pSer282) (kindly provided by Dr. Sakthivel Sadayappan, Department of Cellular & Molecular Medicine, University of Arizona College of Medicine, Tucson, USA, 1:5000), rabbit anti-PDE4D9, goat anti-PDE4B and goat anti-PDE4D (kindly provided by Dr. George Baillie, University of Glasgow, UK, 1:5000). The

blots were washed and incubated with appropriate horseradish peroxidase-conjugated secondary antibodies for 1 h at room temperature. Immunoreactive bands were visualized by ECL western blotting detection kit. Antibody dilutions and exposure times were adjusted to ensure that for each antibody the signal detected was within the linear range. If necessary, membranes were then stripped of bound antibodies by incubation with stripping buffer (Thermo Fisher Scientific, 21059) for 30 min at room temperature with gentle agitation. For western blots analysis, the results from each gel were normalised to the control group from the same gel and the band intensities were quantified by densitometry using ImageJ software.

qPCR

Quantitative PCR was conducted as previously described[13]. In brief, RNA extraction from cardiac tissue was performed using a mixed protocol using phenol:chlorophorm extraction followed by Qiagen RNeasy kits for cleanup. qPCR reactions were perfomed using the ABI Prism 7300 qPCR thermocycler and analysis software (60 °C for 30 s, 95 °C for 10 min followed by 40 cycles of 95 °C for 15 s, 60 °C for 1 min). Reactions were conducted in qPCR Fastmix (VWR, Lutterworth, UK), as previously described. Primers used are as in[13].

Peptide array

Peptide array experiments were performed by automatic SPOT synthesis as described[14-16]. Human TNI peptides were synthesised onto PEG-derivatized continuous cellulose membrane supports *via* 9-fuorenylmethyloxycarbonyl chemistry (Fmoc) using the MultiPep 2 Robot (CEM). A far western blot approach was utilised to detect PDE4D9 (derived from lysate of PDE4D9 overexpressing HEK293 cells), whereby TNI arrays (consisting of 20-25mer peptides) were (i) blocked for 2 h at room temperature in 1X Intercept (TBS) Blocking Buffer (LI-COR), (ii) incubated overnight at 4 °C in [1000 μg] PDE4D9-HEK293 lysate (diluted in 1X TBS, pH 7.4), (iii) incubated overnight at 4 °C in αPDE4D9 rabbit primary antibody (1:1000, bespoke PDE4D9 antibody raised against the unique N-term PDE4D9sequence in rabbits), (iv) incubated for 1 h at room temperature in IRDye 800nm donkey α-rabbit secondary (1:10,000, LI-COR) and (v) visualised *via* Odyssey CLx (LI-COR). Arrays were washed three times in 1X TBS-T following protein, primary and secondary antibody incubation steps. The antibody without lysate was used as a negative control. Antibodies were diluted in 1x Intercept (TBS-T) Antibody Diluent (LIC-COR).

***In vitro* work-loop protocol**

Sprague-Dawley Rats: Sex; Male: Body Mass; 250 – 400g: Number of animals: (5 for P33, 4 for SC, 6 for controls) animals were be purchased from Charles River (Margate, UK) and housed at Warwick University Biomedical Services Unit (BSU) in a 12:12 day/night cycle in rooms held at 22 °C. Cardiac myocytes were isolated as previously described[17]. Isolated cardiac myocyte work-loop experiments were performed using an adapted methods as described previously[18-20]. In brief, myocytes were placed in a perfusion chamber and carefully attached to fine glass rods (high-speed length controller or highly sensitive cantilever force transducer respectively) (IonOptix, Milton, MA, USA). Once attached fresh buffer was cycled through the chamber to remove excess cells. Isometric and force-length protocols were implemented for separate sets of cells incubated in the presence of scrambled or disrupted peptide or DMSO vehicle control. Work-Loop involved electrically stimulating an isometric contraction; the length was held constant until the afterload value was achieved; this was followed by an isotonic phase during which the cell was shortened to maintain a constant level of force. The work-loop protocol was initiated, and the myocytes were paced at 1 Hz using a field stimulator (Myopacer; IonOptix, Milton, MA). Isometric contractions were recorded for 5 min to obtain a baseline/control period. The work-loop protocol relies on the force length relationship and when mimics the cardiomyocyte length change cycle providing realistic evaluation of *in vivo* 'like' myocardial contractile mechanics which involve force feedback work-loops with stepwise preload increases and ramped afterload increases over time. Intervals between loop phases were filled by continuous isometric activations at 1Hz. 2hrs prior to the work-loop experiment and the maximal isometric force (Fmax) and the relaxation velocity were recorded.

Fura-2 measurements

Isolated ARVMs were plated onto laminin (2 μg/cm^2)-coated coverslips and cultured overnight. Cells were loaded with 1 μM Fura-2 AM (Molecular Probes, OR, USA) in the dark at 37°C for 15 min and then washed three times. Coverslips were mounted in the perfusion chamber, continuously perfused with a Tyrode solution containing 1.4 mM Calcium at 37 °C, and paced at 1 Hz using a field stimulator (Myopacer; IonOptix, Milton, MA). When at steady state, cells were perfused with ISO 5 nM for about 10 min. The background-subtracted Fura-2AM

emission at 510 nm was recorded and expressed as a ratio of fluorescent light on excitation at 340 and 380 nm (R340/380). The recorded transients were analysed using the IonWizard software (IonOptix, Milton, MA).

hiPSC-derived cardiac myocytes

Monolayer differentiation of the PGP1 hiPSC cell line[21] was performed via Wnt pathway modulation with small molecule inhibitors. Once stem cell confluence reached ~80%, the cells were induced to form cells of the mesodermal layer with 5μM CHIR99021in RPMI1640/ B27 minus insulin for 24 h. This was day 0 of differentiation. At the end of the 24 h, the medium was replaced with RPMI1640/B27 minus insulin. 48 h later, the medium was replaced with 5 μM IWP2 in RPMI1640/B27 minus insulin for 48 h. Subsequently the medium were replaced with fresh RPMI1640/NB27 minus insulin every 48 h until day 10, when the medium was changed to glucose-free RPMI1640/B27 plus insulin supplemented with 4mM lactate for two 48-h cycles. Spontaneous contraction was observed on day 8-10 of differentiation.

On day 20, iPSC-CMs were dissociated with 10x TrypLE enzyme for 12 min. The dissociation reagent was quenched with plating media (20% fetal bovine serum, 10 μM Thioglycerol in RPMI 1640 supplemented with B27 plus insulin). Cells were collected in suspension, centrifuged at 200 rcf for 3 min and resuspended in plating media. Cardiomyocytes were plated at a density of 1 x 10^6 on Matrigel-coated Ibidi 35mm imaging plates. On day 28 cardiomyocytes were transduced with Adenovirus-RGECO[22]. On day 29, a second transduction was carried out with Adenovirus-α-Actinin-GFP to enable simultaneous Calcium and contractility imaging.

Peptide treatment of iPSC-CMs

On day 30 cardiomyocytes were incubated for 15 min with P33 or scrambled peptide (SC). Controls were provided by equivalent concentrations of dimethylsulfoxide (DMSO). This was repeated in four biological replicates (separate differentiations). A minimum of 30 cells expressing both fluorescent reporters were recorded per plate. Time lapse videos acquired at 1 Hz electrical pacing at 20V and 5msec bipolar current.

Imaging was performed with a Nikon Ti-2 Eclipse inverted microscope (Nikon, Japan) at x100/1.45NA magnification with a Nikon Plan Apo λ (Nikon, Japan). Excitations at 550nm (RGECO) and 470nm (a-Act-GFP) were provided with a CooLED pE4000 (CooLED, UK). Fluorophores were imaged simultaneously using dual illumination through a Quad-Filter (LED-DAPI/FITC/TRITC/Cy5, Semrock, USA). Emissions were passed

through a TwinCam dual camera splitter (Cairn Research, UK), split with a T565lpxr and filtered through an ET632/60 (RGECO) or ET520/40 (GFP) filter (Semrock IDEX, NY, USA). Emissions were collected by two aligned Teledyne Photometrics Kinetix sCMOS cameras (Teledyne Photometrics, USA). Time lapses were acquired at 10 ms exposure (100fps) at 37°C.

Time lapse videos were analysed for Calcium using the published computational pipeline CalTrack[22]. Contractility videos were uploaded into the University of Oxford Advanced Research Computing (ARC) facility cluster and analysed using the automated motion-tracking pipeline SarcTrack[23].

AAV Vector Design and Production

Self-complementary adeno-associated virus serotype 9 (scAAV9) vectors were generated by Vector Biolabs (Malvern, PA, USA). Transgene expression is driven by the cardiac troponin T (cTnT) promoter to ensure cardiomyocyte-specific expression. Two constructs were generated: scAAV9-cTnT-SC-IRES-mCherry-WPRE3 and scAAV9-cTnT-P33-IRES-mCherry-WPRE3. The The SC and P33 inserts encode the sequence of 25 amino acids, using the nucleotide sequences 5'-*ATGAAGACCGA ACTCAAGGCCGAGCGGGGGATCAAGTCCGACGTGGCCAAGGAAAGGGAGCTCCACGACCTGCAGAAGTG A-3'* and 5'-*ATGGGGACCCGGGCCAAGGAATCCTTGGACCTGAGGGCCCACCTCAAGCAG GTGAAGAAGGAGGACATTGAGAAGGAATGA-3'*, respectively. For both vectors, an internal ribosome entry site (IRES) was placed downstream of the primary open reading frame to enable bicistronic expression of mCherry. A WPRE3 element was included to enhance transcript stability and expression efficiency[24,25].

Surgery

All in vivo experiments were approved by the Committee for Animal Care and Ethical Review at the University of Oxford and comply with the UK Animals (Scientific Procedures) Act 1986, as amended 2012. C57BL/6J^{OlaHsd} mice (Envigo, Huntingdon, UK) were group housed in individually ventilated cages under specific pathogen-free conditions at 21 °C with controlled humidity of 55 % and a 13–11 h light-dark cycle.

Water and chow were available ad libitum using irradiated 2016 Teklad Global 16% Protein Rodent Diet. TAC and MI surgery was performed aseptically as described previously[26] under isoflurane general anaesthesia (2% in

medical oxygen with anesthetic depth assessed by loss of pedal reflex)[27]. Buprenorphine analgesia was given subcutaneously immediately prior to surgery (0.8 mg/Kg) and again the morning after surgery (0.4 mg/Kg). TAC surgery was performed in male mice to ensure a consistent hypertrophic response, as female mice exhibit partial protection from pressure overload–induced remodeling due to estrogenic effects[28]. MI surgery was performed in female mice, as male mice showed a higher incidence of sudden cardiac rupture within the first week after surgery (approximately 25 %) compared with females (approximately 5 %), consistent with prior reports. The use of female mice therefore improved postoperative survival and reduced variability in infarct size. All the MI mice were inspected and found to have large infarcts.

Echocardiography and haemodynamics

Mouse transthoracic echocardiography was performed using a Visualsonics Vevo 3100 ultrasound system (Visualsonics, Toronto, Canada) equipped with 22–55 MHz transducer (MS 550D). Mice were maintained on isoflurane anaesthesia (1.0–1.5% in medical O2), placed on a homeothermic table in a supine position. B-mode images were obtained in a parasternal short and long-axis view and dimensions of the left ventricle were measured in a short-axis view in diastole and systole. Diastolic functions were obtained in Apical four-chamber with colour flow imaging for optimal alignment of pulsed-wave Doppler (PWD) and Tissue Doppler imaging (TDI). Data analysis was performed by a single operator blinded to genotype using Vevo Lab, Edition 3.1.1 (Visualsonics, Toronto, Canada). Retrograde LV cannulation was performed under isoflurane anaesthesia via the right carotid artery using a 1.4F solid-state pressure catheter (SPR-839, Millar Instruments, Texas, USA) as described previously[29]. The jugular vein was cannulated using flame-stretch polyethylene tubing (Portex 0.96 mm OD, 800/100/200, Smiths Medical, UK) for administration of dobutamine hydrochloride at 32 ng/g BWt/min. Hearts were removed under anesthesia at the end of the protocol.

Histology

For histological analyses, mouse hearts were harvested and fixed in 4% paraformaldehyde (PFA) at room temperature overnight. For paraffin embedding, samples were dehydrated using a series of graded ethanol concentrations (50-100%, each for at least 2 h), and cleared in butanol overnight. Samples were incubated at 60° C in 1:1 butanol: molten pastillated fibrowax for 30 mins, then three times in 100% molten wax, each for 4 h to

overnight, before embedding and sectioning (10 µm transverse sections). Paraffin sections were stained with the Trichrome Stain Kit (AB150686, Abcam) following the manufacture's protocol. Slides were imaged with a Nanozoomer S210 Slide Scanner (Hamamatsu Photonics, Hamamatsu, Japan) and analyses using Qupath-0.6.0[30].

Human ventricular samples, isolation and culture of human ventricular myocytes

Human ventricular samples were obtained from patients with and without heart failure and reduced ejection fraction at the time of transplantation, valvular surgeries or myectomy and informed consent was obtained from the donors. The study was conducted in accordance with the Declaration of Helsinki and approved by the Ethical Committees of the Aerztekammer Hamburg (WF-088/18). After surgical excision, tissue samples were placed into Custodiol® solution (Dr. Franz Köhler Chemie GmbH) and transported to the laboratory. Of the 26 samples obtained, 10 were used for western blot (Extended Data table 6), and 16 for myocytes isolation (Extended Data table 5). Human ventricular myocytes were isolated as previously described (doi: 10.1093/eurheartj/ehad086). Briefly, tissue was cut into small pieces and digested in Stop Ca^{2+} free solution (containing in mM: 88 Sucrose, 88 NaCl, 5.4 KCl, 4 NaHCO3, 0.3 NaH2PO4, 1.1 MgCl2, 10 HEPES, 20 Taurine, 10 Glucose, 5 Na+ pyruvate. 7.4 pH at room temperature; 5% BSA, and 12 µM blebbistatin) plus 0.5 mg ml-1 collagenase (Worthington type 1, 240 U), 0.5 mg ml-1 proteinase (Sigma type XXIV, 11 U) and 2% bovine serum albumin (BSA; Sigma, St. Louis, Missouri, USA) by spinning it at 200 rpm and 37 °C 30 min. Then tissues were transferred to Stop Ca^{2+} free solution alone and moved up and down in a Pasteur pipette for mechanical dissociation. The remaining tissue was digested for 5 more rounds in Stop Ca^{2+} free solution with 0.4 mg ml-1 collagenase and 2% BSA at 200 rpm and 37 °C 15 min, until the tissue was completely digested. Human ventricular myocytes were harvested by centrifugation at 500 rpm during 5 min and resuspended in MEM medium (M 4780; Sigma-Aldritch) containing 2 mmol/L Ca^{2+}, 2.5% fetal bovine serum (FBS, Invitrogen), 1% penicillin-streptomycin and 12 µM blebbistatin. Myocytes were then plated on Laminin-coated dishes (Cellvis). After 2 h at 37 °C and 5% CO_2, medium was changed to FBS-free MEM medium containing adenovirus (MOI 200 PFU/cell) and keep them in culture at 37°C and 5% CO_2 until FRET experiments were performed 24-48 h after.

Statistical analysis

Statistical analyses were performed using GraphPhPad Prism 10. For western blots analysis, the results from each gel were normalised to the control group from the same gel. One-way ANOVAs with *post* hoc test, paired or unpaired two-tailed Student's t-tests were used as appropriate. Welch correction was applied as indicated. Statistical significance was defined as $P < 0.05$ with a 95% confidence interval. When providing summary statistics, X ± Y represents the mean (X) and standard deviation (Y). For experiments using human cardiomyocytes, data are expressed as (*x/y*), where *x* denotes the total number of individual cells analyzed and *y* denotes the number of independent patient-derived samples. Each patient (*y*) represents one biological replicate, and multiple cells (*x*) were analyzed per sample.

Results

Distinct cAMP regulation at TPNI. We first sought to confirm whether TPNI designates a nanodomain at the myofilament where cAMP is uniquely regulated. For this, we used the FRET-based cAMP reporter TPNI-CUTie[6] and the newly developed MyBPC-CUTie (Fig. 1a,b) to monitor the cAMP signal at TPNI and MyBPC, a PKA target proximal to TPNI on the myofilaments (Fig. 1b). Correct localisation of TPNI-CUTie and MyBPC-CUTie was confirmed by co-immunoprecipitation and immunostaining (Fig. 1c-e). Overlapping kinetics and maximal amplitudes of the cAMP-dependent FRET changes at saturating cAMP (Fig. 1f) allowed direct comparison of the FRET change reported by the two sensors. Adult rat ventricular myocytes (ARVM) expressing TPNI-CUTie, MyBPC-CUTie or the previously characterised AKAP18δ -CUTie[6], a sensor targeted to the SR and forming a complex with PLB and SERCA (Fig. 1b,c), were then challenged with the β-AR agonist isoproterenol (ISO, 5nM). Consistent with our previous findings[6], the cAMP response at AKAP18δ was faster, significantly larger and sustained for at least 5 min compared to the cAMP response at TPNI, where cAMP elevation was slower and transient, peaking at 1 min after addition of ISO and returning close to baseline after 5 min (Fig. 1g,h). Remarkably, the cAMP response at MyBPC was also distinct, with maximal amplitude and velocity similar to TPNI at 1 min but with sustained kinetics for at least 5 min (Fig. 1g,h). Similar differences were confirmed in neonatal rat ventricular myocytes (NRVM) (Extended Data Fig. 1). The divergence in cAMP kinetics was

reflected in the time course of PKA-dependent phosphorylation, with TPNI phosphorylation peaking at about 5 min after the application of 5 nM ISO and declining significantly after 10 min, whereas phosphorylation of MyBPC and PLB showed a steady increase up to 10 min after ISO application (Fig. 1i-j). Thus, β-AR activation generates a cAMP signal at TPNI that is transient in nature and clearly distinct from the signal generated at the SERCA/PLB complex and at MyBPC, despite the close proximity of these targets.

A PDE4D uniquely modulates cAMP at TPNI. We previously demonstrated that the transient cAMP response to ISO at TPNI is abolished in the presence of the non-selective PDE inhibitor 3-isobutyl-1-methylxanthine (IBMX), resulting in a sustained elevation of the second messenger at this site[6]. Proteomic studies indicate that both PDE2A and PDE3A isoforms are associated with cardiac myofilaments[31]. To assess whether either of these enzyme families is responsible for the unique transient nature of the cAMP signal at TPNI, NRVM expressing TPNI-CUTie or MyBPC-CUTie were treated with 1 nM ISO and either the PDE2A inhibitor BAY 60-7550 (BAY, 10 nM) or the PDE3 inhibitor cilostamide (Cilo, 10 μM), and local cAMP levels recorded over time. Elevation of the FRET signal on inhibitor application indicates that both PDE2A and PDE3A contribute to cAMP hydrolysis at both locations (Fig. 2a,b,e). However, both inhibitors failed to eliminate the transient nature of the response at TPNI (Fig. 2a,b,e), even upon simultaneous inhibition of the two enzymes (Fig. 2c). By contrast, inhibition of PDE4 with rolipram (Roli 10 μM) resulted in a sustained response at TPNI (Fig. 2d,e), indicating a PDE4 isoform is the main determinant of the transient cAMP elevation at this location.

Of the four PDE4 families (PDE4A, PDE4B, PDE4C, and PDE4D), PDE4B and PDE4D are the most abundantly expressed in rat cardiac myocytes[32]. To identify the PDE4 subfamily involved, small interference RNA was applied to NRVM to knock down (KD) either PDE4B or PDE4D subfamilies[33] (Extended Data Fig. 2). While the cAMP response to ISO at TPNI was not affected by PDE4B KD, PDE4D KD resulted in a sustained response (Fig. 2f).

Given the extremely localised nature of the cAMP regulation at TPNI, we next investigated whether a PDE4D enzyme might be in a complex with TPNI. Immunoprecipitation of TPNI from ARVMs co-precipitated PDE4D enzymes with a molecular weight consistent with PDE4D9 (Fig. 2g). As PDE4D9 migrates at a similar size as

PDE4D3 and PDE4D8[34], we used quantitative PCR to distinguish between them and found tha PDE4D9 is the most abundantly expressed in NRVMs (Extended Data Fig. 3). We therefore focused our subsequent analyses on this enzyme. To confirm that PDE4D9 operates at TPNI, we expressed a catalytically inactive mutant of PDE4D9 in NRVM. This mutant acts as a dominant-negative (DN) construct that displaces the native enzyme from its anchoring sites, thereby enhancing ISO-induced cAMP signaling at the location where the endogenous enzyme is normally localised[35]. As shown in Fig. 2h, expression of PDE4D9-DN resulted in a larger and sustained cAMP response to ISO at TPNI relative to control, while no significant difference was observed at MyBPC (Fig. 2i). Notably, we found that the amount of PDE4D9 detected in the TPNI immunoprecipitate was dependent on the extent of β-AR activation (Fig. 2j).

PDE4D9 directly interacts with TPNI. To confirm direct interaction of TPNI with PDE4D9 and to explore the interacting surface, we used peptide array technology[36]. TPNI arrays consisting of 20- (Extended Data Fig. 4a) or 25-mers (not shown) covering the entire sequence of rat TPNI, were probed with purified GST-tagged PDE4D9. A strong interaction was found for several peptides that were further analysed by alanine scanning, where each of the amino acids in the selected peptide was substituted with alanine or, if originally an alanine, with glycine. Peptide alanine scanning of peptide 33 from the original array identified lysine residues at position K175, K178, K179 (Extended Data Fig. 4b) and K184 (not shown) as required for interaction with GST-PDE4D9. Interestingly, a lysine to glutamate mutation at position 178 of human TPNI (corresponding to rat K179), causes an inherited restrictive cardiomyopathy[37]. To confirm the role of this residue in the TPNI/PDE4D9 interaction, we introduced the K178E mutation in TPNI-CUTie ($TPNI_{K178E}$-CUTie) (Extended Data Fig. 5a,b) and probed the ability of the mutated TPNI moiety in this sensor to interact with PDE4D9 compared to TPNI-CUTie. As shown in Extended Data Fig. 5c, the K178E mutation significantly reduced the interaction with and, when used to measure cAMP levels, $TPNI_{K178E}$-CUTie detected a significantly larger and sustained cAMP signal in response to ISO stimulation compared to TPNI-CUTie (Extended Data Fig. 5d). Comparable results were obtained using a TPNI-CUTie mutant ($TPNI_{mut}$-CUTie) carrying the mutations K177A, K178A and K183A (corresponding to rat K184) (Extended Data Fig. 5a-d). Consistently, ISO treatment of NRVM expressing $TPNI_{mut}$-CUTie resulted in sustained phosphorylation of the TPNI moiety, in clear contrast to the transient phosphorylation of TPNI-CUTie

(Extended Data Fig. 5e). Collectively, the data show that a carboxyl-terminal region of TPNI encompassing K177-K183 interacts with PDE4D9, and the TPNI peptide P33, with sequence G_{161}TRAKESLDLRAHLKQVKKEDIEKE$_{185}$ (Extended Data Fig. 5f), was selected for further studies.

P33 selectively boosts local cAMP levels and phosphorylation of TPNI. We next assessed whether P33 can displace PDE4D9 from TPNI in cardiac myocytes. Pre-treatment of isolated NRVM with stearylated P33 (10 μM) for 2 h significantly reduced TPNI/PDE4D9 co-immunoprecipitation compared to treatment with a control peptide with scrambled amino acid sequence (SC, 10 μM), both in unstimulated cells and upon ISO stimulation (Fig. 3a,b). Consistently, cAMP levels measured in NRVM expressing TPNI-CUTie and pre-treated with P33 showed increased amplitude and duration of the cAMP signal compared to cells pretreated with vehicle DMSO or SC peptide (Fig. 3c). The effect of P33 is highly specific for TPNI, as no difference in the cAMP response between SC and P33 pre-treatment was observed at MyBPC (Fig. 3d) or AKAP18δ (Fig. 3e), where the response at 5 min was significantly higher than at 1 min upon either treatment and no different from DMSO control. Consistently, treatment with P33 resulted in a sustained phosphorylation of TPNI in response to ISO, while it had no effect on the phosphorylation of MyBPC or PLB (Fig 3f-g).

In cardiac myocytes differentiated from human inducible pluripotent stem cells (hiPSC-CM), where the level of TPNI phosphorylation in response to ISO stimulation also showed a transient elevation (Extended Data Fig. 6a), treatment with P33 significantly enhanced TPNI phosphorylation (Extended Data Fig. 6b) and significantly reduced TPNI/PDE4D9 interaction (Extended Data Fig. 6c,d) compared to treatment with SC control.

Treatment with P33 did not affect the cAMP response to ISO measured at the plasmalemma using the targeted AKAP79-CUTie sensor[6] (Extended Data Fig. 7a,b), or in the bulk cytosol using the untargeted cytosolic CUTie sensor[6] (Extended Data Fig. 7c,d). Moreover, P33 had no impact on global PDE4 or PDE activity, as measured with the cytosolic cAMP sensor EPAC-H187[38] upon application of rolipram (10 μM) or IBMX (100 μM), respectively (Extended Data Fig. 7e,f).

P33 enhances relaxation and contraction *in vitro*. Given the observed effect of displacing PDE4D9 with P33 on TPNI phosphorylation, we expected treatment with P33 to enhance relaxation and force generation[39-43]. To verify

this, we measured the velocity of relaxation using a work-loop technique in single isolated ARVM upon pacing at 1Hz[19,20]. We measured an average 2.2-fold increase (149.07 ± 89.90 for P33 vs 67.00 ± 31.29 for SC) in relaxation velocity in samples treated with P33 compared to SC (Fig. 3h). This was accompanied by an average 2.1-fold increase (183.23 ± 114.26 for P33 vs 84.77 ± 48.66 for SC) in isometric contractile force (Fig. 3h). When P33 was used to pre-treat hiPSC-CM, we found enhanced sarcomere length at relaxation (Extended Data Fig. 8a) and enhanced contraction (Extended Data Fig. 8b). Notably, the effects of P33 on lusitropy and force generation were independent of changes in the amplitude and duration of the Calcium transient (Fig. 3i, Extended Data Fig. 8c-i and Extended Data Fig. 9).

Aberrant PDE4D9/TPNI interaction in cardiac disease. Defective phosphorylation of TPNI has been reported in animal models of cardiac disease[44-47] and in patients suffering from cardiomyopathies[48-51], although the underlying aetiology remains unclear. We therefore explored whether the novel mechanism we uncovered for the selective regulation of TPNI phosphorylation may be altered in disease. We found 2.9-fold more PDE4D9 associated with TPNI in unstimulated cells obtained from failing cardiac myocytes from a mouse model of myocardial infarction (MI) compared to sham controls (Fig. 4a,b). Consistently, and in line with previous reports, we found attenuated TPNI phosphorylation compared to cells from age-matched healthy controls, while no difference was found in the phosphorylation of MyBPC (Fig. 4c,d). We also found a 5.1-fold larger amount of PDE4D9 interacting with TPNI in cardiac myocytes from a mouse surgical model of transverse aortic constriction (TAC) (Extended Data table 1 and Fig. 4e,f), relative to sham control.

P33 disrupts the TPNI/PDE4D9 interaction *in vivo*. To test whether P33 may attenuate diastolic dysfunction *in vivo*, we designed a self-complementary recombinant adeno-associated virus[52] carrying the sequence for the control SC (scAAV9-SC) or P33 (scAAV9-P33) peptides followed by the coding sequence for mCherry under the control of an internal ribosome entry site (IRES) (Extended Data Fig. 10a). Expression of both constructs in healthy mice was confirmed by detection of mCherry in cardiac myocytes isolated 3 weeks after tail vein injection of 10^{12} vector particles (Extended Data Fig. 10b). In the same cells, efficient expression of P33 was confirmed by a 60% reduction in the amount of PDE4D9 co-immunoprecipitated with TPNI in cardiac myocytes from mice injected with scAAV9-P33 compared to scAAV9-SC (Extended Data Fig. 10c). Consistently, we found a 2-fold

increase in TPNI phosphorylation in mice injected with scAAV9-P33 compared to scAAV9-SC (Extended Data Fig. 10d). Compared to scAAV9-SC, injection of scAAV9-P33 did not affect overall cardiac performance as assessed by echocardiography (Extended Data table 2 and Extended Data Fig. 11) and LV haemodynamic (Extended Data table 3) at 3 weeks post-injection, but resulted in a 1.3-fold elevation (0.98 ± 0.26 for SC vs 1.29 ± 0.10 for P33) of E'/A' (Extended Data Fig 11c), indicating enhanced relaxation.

P33 improves diastolic function *in vivo*. To test whether P33 protects from the development of diastolic dysfunction, a cohort of mice were TAC or sham operated and, 1 week after surgery, tail vein injected with 10^{12} scAAV9- or scAAV9-P33 vector particles. Three weeks after injection, the cardiac phenotype was studied (Fig. 5a, Extended Data table 4). A 3.5-fold increase (3.04 ± 2.11 for sham SC vs 10.91 ± 2.53 for TAC SC) in fibrosis was observed in TAC compared to sham operated mice injected with scAAV9-SC, which was limited to a 1.7-fold increase (5.40 ± 2.28 for TAC P33) in TAC mice injected with scAAV9-P33 (Fig. 5b,c). Elevated LV weight normalised to tibial length (Fig. 5d), without evident increase in lung weight (Fig. 5e) in the TAC-SC group compared to sham-SC, indicates robust cardiac hypertrophy, in the absence of pulmonary congestion (Fig. 5e). A trend for diastolic LV dilatation (Fig. 5f) along with a 30% lower (72 ± 8.8 for sham SC vs 50 ± 12.3 for TAC SC) ejection fraction in TAC-SC compared to Sham-SC (Fig. 5g), indicated contractile dysfunction consistent with early-stage HF. Injection of scAAV9-P33 resulted in 30% reduction in LV hypertrophy (7.76 ± 1.24 for TAC SC vs 6.34 ± 0.74 for TAC P33, Fig. 5d) and acted to preserve ejection fraction (Fig. 5g). A 1.4-fold elevation (31.54 ± 9.12 for sham SC vs 45.84 ± 10.27 for TAC SC) of E/e' in TAC mice treated with SC, suggesting an increase in diastolic filling pressure, was reduced to a 0.1-fold increase (36.70 ± 4.73 for TAC P33) in P33 treated mice (Fig. 5h). LV haemodynamic measurements (Extended Data table 5) confirmed the beneficial effect of P33 in TAC mice. As expected, LV end-systolic pressure was greatly elevated in both TAC groups, although to a slightly lesser extent in P33 treated mice (Fig. 5j). The same difference was not observed upon maximal β-adrenergic stimulation with dobutamine (Fig. 5o), suggesting it was not due to divergence in the surgical placement of the aortic band. Treatment with P33, but not SC, completely normalized LV end-diastolic pressure (Fig. 5k), in keeping with the echocardiographic E/e' findings (Fig. 5h). Baseline values for the maximal rate of pressure rise (dP/dtmax) were not significantly different between groups, however, this parameter is

sensitive to preload, so an elevated LVEDP in the TAC-SC group may have maintained a deceptively high dP/dt_{max}. The time constant of isovolumetric relaxation (tau) was prolonged by 1.6-fold (7.2 ± 1.4 for sham SC vs 11.8 ± 2.3 for TAC SC) in the TAC-SC group but to a lesser extent (1.4-fold, 9.9 ± 2.30 for TAC P33) in the TAC-P33 group (Fig. 5m). The beneficial effect of P33 remained evident when mice were subjected to dobutamine stress (32 ng/g BW/min), with complete normalisation of LVEDP (Fig. 5p) and normal values for tau (Fig. 5r). Notably, all groups were capable of increasing dP/dt_{max} upon dobutamine stimulation, indicating that P33 treatment did not blunt contractile reserve (Fig. 5q versus Fig. 5l).

Mechanistically, the beneficial effect of P33 is explained by the finding that treatment with P33 of TAC animals reduced by 40% the interaction of PDE4D9 with TPNI compared to SC peptide treatment (Fig. 5s), resulting in a 2.8-fold increase in TPNI phosphorylation (Fig. 5t). By contrast, no effect on MyBPC phosphorylation was detected in SC or P33 treated TAC animals compared to sham (Fig. 5t).

Translational applications of P33. While humans display a much slower heart rate than mice, simulations of excitation-contraction coupling using T-World[53], a state-of-the-art virtual human cardiomyocyte, confirm a robust effect of displacing PDE4 from TPNI and normalization of diastolic function on disruption of PDE4/TPNI interaction, supporting a beneficial effect also at human-relevant heart rates (Extended Data Fig. 12 and supplemental information).

Unlike rodents, human cardiac myocytes express predominantly PDE3 and relatively less PDE4 isoforms[54]. To confirm a role of PDE4 isoforms in the regulation of cAMP at TPNI in human cardiac myocytes, we compared, in myocytes obtained from HF patients (Extended Data table 6), the cAMP response on inhibition of PDE4 with Roli in the bulk cytosol, using the untargeted cAMP reporter Epac-1[55], and at the troponin complex, using the TPNI-CUTie sensor (Fig. 6a). As expected, we found that the contribution of PDE4 isoforms to the regulation of bulk cytosolic cAMP is modest (Fig. 6b). By contrast, PDE4 inhibition had a more prominent effect (4.3-fold larger on average, 8.93 ± 7.66 for bulk cytosol vs 38.42 ± 21.76 for TPNI) on the cAMP response measured at TPNI (Fig. 6b). Similar to that was observed in rodent myocytes, the cAMP response to ISO (1 nM) was sustained at MyBPC but transient at TPNI (Fig. 6c), where subsequent inhibition of PDE4 led to a sustained elevation (Fig. 6c). As previously reported, analysis of left ventricular tissue from HF patients (Extended Data

table 7) confirmed that TPNI phosphorylation is significantly reduced in failing hearts relative to healthy controls (Fig. 6d-e, Extended Data table 7). Notably, and consistent with our observations in rodents, this phosphorylation defect is explained by a prominent increase (1.8-fold on average) in the amount of PDE4D9 interacting with TPNI in HF patients relative to healthy controls, as revealed by co-immunoprecipitation experiments (Fig. 6f-g). To assess the potential beneficial effect of displacing PDE4D9 from TPNI in HF patients, we pre-treated human ventricular myocytes isolated from HF samples with 10 μM of either P33 or SC peptide for 2 h. At this time point we measured the effect on the local level of cAMP using TPNI-CUTie at 0.5 and 5 min after addition of 5 nM ISO and found a significantly larger cAMP response in P33-treated myocytes compared to SC control (Fig. 6h).

Discussion. Heart failure remains a major global health challenge, contributing substantially to morbidity, mortality, and healthcare costs worldwide[56]. Limited understanding of HF pathophysiology has so far hampered development of therapeutics that target the molecular mechanisms underpinning this condition[57]. This is particularly true for diastolic dysfunction, for which current medications are often ineffective[58]. Individuals with diastolic dysfunction face a 2–3-fold higher risk of symptomatic heart failure and a 50–60% greater risk of all-cause mortality compared with those with normal diastolic function[59,60]. Despite this substantial burden, no pharmacologic therapy currently improves diastolic function or reduces the associated mortality[61]. Extensive evidence indicates that the contractile apparatus exhibits heightened sensitivity to Calcium in end-stage HF[48,51,62], making a strong case for targeting myofilament Calcium sensitivity for therapeutic purposes. However, proposed interventions[63-66] are encumbered by lack of specificity and technical complexity[65,67].

Here, we discovered a novel mechanism that modulates Calcium sensitivity by precisely regulating cAMP/PKA-dependent phosphorylation of TPNI with nanometer subcellular precision. This mechanism involves the direct interaction of PDE4D9 with TPNI, leading to localized cAMP degradation and reduced TPNI phosphorylation by PKA. The action range of the TPNI-anchored PDE4D9 is tightly confined, with its hydrolytic activity becoming ineffective beyond approximately 30 nm from the TPNI/PDE4D9 complex, where MyBPC is localised. Our findings align with the current understanding that cAMP signalling is highly compartmentalized and functions through the formation of localized signalling domains. In these structures, PKA is anchored near specific targets

and is activated by confined pools of cAMP. Although not directly addressed in this study, TPNT is the likely local docking site for PKA, as it has been reported to function as an AKAP[68].

We demonstrate that, by selectively displacing PDE4D9 from TPNI, the highly localized nature of this regulatory mechanism can be leveraged to achieve local elevation of cAMP, local activation of PKA, and selective phosphorylation of TPNI. As expected, this phosphorylation promotes cardiac myocyte relaxation, as seen in isolated cells. Consistently, we also observed enhanced inotropy, likely due to increased crossbridge cycling rate and shortening velocity[39-41,69]. Importantly, these effects extend *in vivo*, where displacement of PDE4D9 from TPNI normalises ventricular end-diastolic pressure and improves ejection fraction in a mouse TAC model of heart failure.

A key advantage of locally elevating cAMP by displacing PDE4D9 from the myofilament is the exquisite selectivity of this intervention, both at the cellular and subcellular level. TPNI expression is confined to striated muscle and PKA phosphorylates TPNI exclusively in cardiac myocytes. Thus, the effects of disrupting the TPNI/PDE4D9 interaction are expected to be highly specific to cardiac myocytes. The same targeted effect of displacing PDE4D9 from TPNI could not be achieved pharmacologically, as available PDE4 inhibitors are not isoform-selective, and would inhibit all the 25 PDE4 isoforms simultaneously, both in cardiac myocytes and other tissues. We demonstrate that, instead, elevating cAMP through PDE4D9 displacement from TPNI does not affect the overall hydrolytic activity of PDE4 or other PDEs in the cell, potentially avoiding off-target effects. Moreover, displacing PDE4D9 from TPNI does not affect local cAMP signalling at the AKAP79-L-type Calcium channel complex at the plasmalemma or at the AKAP18δ-SERCA/PLB complex at the SR, supported by the fact that treatment with P33 has no effect on the amplitude of the Calcium transient. Thus, unlike treatments that globally elevate cAMP in the cell, this selective displacement is expected to offer the additional benefit of improving cardiac performance without increasing SERCA activity and, consequently, ATP consumption. As evidenced by the response under dobutamine stress, it also preserves cardiac reserve, which instead is lowered by β-blockers.

The observation that the expression of PDE4D isoforms is elevated in human failing hearts is exciting and can explain the defective phosphorylation of TPNI widely reported in cardiac patients[48-51]. While PDE4 isoforms are

relatively less abundant than PDE3 isoforms in human cardiac myocytes, we show that they significantly contribute to the regulation of cAMP at TPNI, and that displacement of PDE4D9 from TPNI with the disrupting peptide P33 results in local elevation of cAMP in human ventricular myocytes.

Currently, no effective treatment exists that selectively targets the mechanisms underpinning myofilament relaxation[70]. The high morbidity and mortality associated with diastolic dysfunction make this a major unmet medical need worldwide[4]. Our work indicates that targeting PDE4D9 displacement from the myofilament may provide a new, mechanism-based avenue for the treatment of heart disease. More broadly, it lays the foundation for the development of precision therapeutics in other organ systems where cAMP compartmentalisation orchestrates cellular function.

Disclosure statement

M.Z., Y-C.C. and J.H. have filed for a patent on a peptide for treating heart failure (UK Patent Application Number 2507142.4).

Acknowledgements

M.Z acknowledges funding by the British Heart Foundation (RG/12/3/29423, RG/17/6/32944, PG/23/11321, PG/21/10611), the Oxford BHF Centre of Research Excellence by grant code (RE/08/004, RE/18/3/34214) and the Oxford NIHR Biomedical Research Centre. C.E.M. acknowledges funding by the Deutsche Forschungsgemeinschaft (ES 569/2-2 and ES 569/3-1), the Gertraud und Heinz-Rose Foundation and the German Centre for Cardiovascular Research (DZHK). The work-loop experiments were supported by InoCardia Ltd and Coventry University. C.L. acknowledges funding from British Heart Foundation grant (RG/18/12/34040).

Author contributions

Y-C.C. and M.Z. designed the study, with M.Z. supervising the overall project and acquiring funding. Experimental work included imaging experiments performed by Y-C.C., W-H.H., E.V., M.G.O., A.K., N.C.S., J.H., M.F.; biochemical work performed by Y-C.C., R.Y., M.G.O.; qPCR experiments were conducted by D.H.; in vitro work-loop experiments were conducted by J.H., A.L. and H.M.; peptide arrays were conducted by H.S, C.B. and G.B; work related to in vivo animal models was designed by C.L. and carried out by D.J.M, C.L., Y-C.C. and J.G.; work using hiPSC-derived cardiomyocytes was carried out by Y.P. and C.T.; histological analyses were conducted by W-H.H. and N.S.; the modelling was carried out by J.T.; work with human ventricular myocytes was carried out by D.R, E.G. and C.E.M; Y-C.C. and MZ wrote the manuscript.

Additional information

Supplementary Information is available for this paper. Correspondence and requests for materials should be addressed to Manuela Zaccolo (manuela.zaccolo@dpag.ox.ac.uk)

References

1 Bers, D. M. Cardiac excitation-contraction coupling. *Nature* **415**, 198–205 (2002). https://doi.org/10.1038/415198a

2 Bristow, M. R. *et al.* Decreased catecholamine sensitivity and beta-adrenergic-receptor density in failing human hearts. *N Engl J Med* **307**, 205–211 (1982). https://doi.org/10.1056/NEJM198207223070401

3 Neubauer, S. The failing heart--an engine out of fuel. *The New England journal of medicine* **356**, 1140–1151 (2007). https://doi.org/10.1056/NEJMra063052

4 Mishra, S. & Kass, D. A. Cellular and molecular pathobiology of heart failure with preserved ejection fraction. *Nat Rev Cardiol* **18**, 400–423 (2021). https://doi.org/10.1038/s41569-020-00480-6

5 Zaccolo, M. & Kovanich, D. Nanodomain cAMP signalling in cardiac pathophysiology: potential for developing targeted therapeutic interventions. *Physiol Rev* (2024). https://doi.org/10.1152/physrev.00013.2024

6 Surdo, N. C. *et al.* FRET biosensor uncovers cAMP nano-domains at beta-adrenergic targets that dictate precise tuning of cardiac contractility. *Nat Commun* **8**, 15031 (2017). https://doi.org/10.1038/ncomms15031

7 Scott, J. D. & Santana, L. F. A-kinase anchoring proteins: getting to the heart of the matter. *Circulation* **121**, 1264–1271 (2010).

8 Kamel, R., Leroy, J., Vandecasteele, G. & Fischmeister, R. Cyclic nucleotide phosphodiesterases as therapeutic targets in cardiac hypertrophy and heart failure. *Nat Rev Cardiol* **20**, 90–108 (2023). https://doi.org/10.1038/s41569-022-00756-z

9 Kokkonen, K. & Kass, D. A. Nanodomain Regulation of Cardiac Cyclic Nucleotide Signaling by Phosphodiesterases. *Annual review of pharmacology and toxicology* **57**, 455–479 (2017). https://doi.org/10.1146/annurev-pharmtox-010716-104756

10 Lomas, O. *et al.* Adenoviral transduction of FRET-based biosensors for cAMP in primary adult mouse cardiomyocytes. *Methods Mol Biol* **1294**, 103–115 (2015). https://doi.org/10.1007/978-1-4939-2537-7_8

11 Zaccolo, M. & Pozzan, T. Discrete microdomains with high concentration of cAMP in stimulated rat neonatal cardiac myocytes. *Science* **295**, 1711–1715 (2002).

12 Stangherlin, A. *et al.* cGMP signals modulate cAMP levels in a compartment-specific manner to regulate catecholamine-dependent signaling in cardiac myocytes. *Circ Res* **108**, 929–939 (2011). https://doi.org/10.1161/CIRCRESAHA.110.230698

13 Henderson, D. J. *et al.* The cAMP phosphodiesterase-4D7 (PDE4D7) is downregulated in androgen-independent prostate cancer cells and mediates proliferation by compartmentalising cAMP at the plasma membrane of VCaP prostate cancer cells. *Br J Cancer* **110**, 1278–1287 (2014). https://doi.org/10.1038/bjc.2014.22

14 Cooke, S. F. *et al.* Disruption of the pro-oncogenic c-RAF-PDE8A complex represents a differentiated approach to treating KRAS-c-RAF dependent PDAC. *Sci Rep* **14**, 8998 (2024). https://doi.org/10.1038/s41598-024-59451-3

15 Brown, K. M. *et al.* Phosphodiesterase-8A binds to and regulates Raf-1 kinase. *Proc Natl Acad Sci U S A* **110**, E1533–1542 (2013). https://doi.org/10.1073/pnas.1303004110

16 Amartely, H., Iosub-Amir, A. & Friedler, A. Identifying protein-protein interaction sites using peptide arrays. *J Vis Exp*, e52097 (2014). https://doi.org/10.3791/52097

17 Maddock, H. L., Mocanu, M. M. & Yellon, D. M. Adenosine A(3) receptor activation protects the myocardium from reperfusion/reoxygenation injury. *American journal of physiology. Heart and circulatory physiology* **283**, H1307–1313 (2002). https://doi.org/10.1152/ajpheart.00851.2001

18 Tran, P. *et al.* Profiling the Biomechanical Responses to Workload on the Human Myocyte to Explore the Concept of Myocardial Fatigue and Reversibility: Rationale and Design of the POWER Heart Failure Study. *J Cardiovasc Transl Res* **17**, 275–286 (2024). https://doi.org/10.1007/s12265-023-10391-9

662 19 Gharanei M, B. M., Linekar A, Wallis R, Chuizbaian O, Maddock H. . Development of an in vitro platform
663 using the human primary cardiomyocyte work loop assay to screen for drug-induced effects on cardiac
664 contractility. *Journal of Pharmacological and Toxicological Methods* **93** (2018).
665 https://doi.org/10.1016/j.vascn.2018.01.428
666 20 Helmes, M. *et al.* Mimicking the cardiac cycle in intact cardiomyocytes using diastolic and systolic force
667 clamps; measuring power output. *Cardiovasc Res* **111**, 66–73 (2016).
668 https://doi.org/10.1093/cvr/cvw072
669 21 Margara, F. *et al.* Mechanism based therapies enable personalised treatment of hypertrophic
670 cardiomyopathy. *Sci Rep* **12**, 22501 (2022). https://doi.org/10.1038/s41598-022-26889-2
671 22 Psaras, Y. *et al.* CalTrack: High-Throughput Automated Calcium Transient Analysis in Cardiomyocytes. *Circ*
672 *Res* **129**, 326–341 (2021). https://doi.org/10.1161/CIRCRESAHA.121.318868
673 23 Toepfer, C. N. *et al.* SarcTrack. *Circ Res* **124**, 1172–1183 (2019).
674 https://doi.org/10.1161/CIRCRESAHA.118.314505
675 24 Zufferey, R., Donello, J. E., Trono, D. & Hope, T. J. Woodchuck hepatitis virus posttranscriptional
676 regulatory element enhances expression of transgenes delivered by retroviral vectors. *J Virol* **73**, 2886–
677 2892 (1999). https://doi.org/10.1128/JVI.73.4.2886-2892.1999
678 25 Choi, J. H. *et al.* Optimization of AAV expression cassettes to improve packaging capacity and transgene
679 expression in neurons. *Mol Brain* **7**, 17 (2014). https://doi.org/10.1186/1756-6606-7-17
680 26 Lygate CA, N. S. Surgically induced chronic heart failure. **A Handbook of Mouse Models of**
681 **Cardiovascular Disease**, 333–348 (2006).
682 27 Lygate, C. A. *et al.* Serial high resolution 3D-MRI after aortic banding in mice: band internalization is a
683 source of variability in the hypertrophic response. *Basic Res Cardiol* **101**, 8–16 (2006).
684 https://doi.org/10.1007/s00395-005-0546-3
685 28 Fliegner, D. *et al.* Female sex and estrogen receptor-beta attenuate cardiac remodeling and apoptosis in
686 pressure overload. *Am J Physiol Regul Integr Comp Physiol* **298**, R1597–1606 (2010).
687 https://doi.org/10.1152/ajpregu.00825.2009
688 29 Faller, K. M. E. *et al.* Impaired cardiac contractile function in arginine:glycine amidinotransferase
689 knockout mice devoid of creatine is rescued by homoarginine but not creatine. *Cardiovasc Res* **114**, 417–
690 430 (2018). https://doi.org/10.1093/cvr/cvx242
691 30 Bankhead, P. *et al.* QuPath: Open source software for digital pathology image analysis. *Sci Rep* **7**, 16878
692 (2017). https://doi.org/10.1038/s41598-017-17204-5
693 31 Subramaniam, G. *et al.* Integrated Proteomics Unveils Nuclear PDE3A2 as a Regulator of Cardiac Myocyte
694 Hypertrophy. *Circ Res* **132**, 828–848 (2023). https://doi.org/10.1161/CIRCRESAHA.122.321448
695 32 Mongillo, M. *et al.* Fluorescence resonance energy transfer-based analysis of cAMP dynamics in live
696 neonatal rat cardiac myocytes reveals distinct functions of compartmentalized phosphodiesterases. *Circ*
697 *Res* **95**, 67–75 (2004).
698 33 Li, X., Huston, E., Lynch, M. J., Houslay, M. D. & Baillie, G. S. Phosphodiesterase-4 influences the PKA
699 phosphorylation status and membrane translocation of G-protein receptor kinase 2 (GRK2) in HEK-
700 293beta2 cells and cardiac myocytes. *Biochem J* **394**, 427–435 (2006).
701 https://doi.org/10.1042/BJ20051560
702 34 Richter, W., Jin, S. L. & Conti, M. Splice variants of the cyclic nucleotide phosphodiesterase PDE4D are
703 differentially expressed and regulated in rat tissue. *Biochem J* **388**, 803–811 (2005).
704 https://doi.org/10.1042/BJ20050030
705 35 McCahill, A. *et al.* In resting COS1 cells a dominant negative approach shows that specific, anchored
706 PDE4 cAMP phosphodiesterase isoforms gate the activation, by basal cyclic AMP production, of AKAP-
707 tethered protein kinase A type II located in the centrosomal region. *Cell Signal* **17**, 1158–1173 (2005).
708 36 Tibbo, A. J. *et al.* Phosphodiesterase type 4 anchoring regulates cAMP signaling to Popeye domain-
709 containing proteins. *J Mol Cell Cardiol* **165**, 86–102 (2022). https://doi.org/10.1016/j.yjmcc.2022.01.001

710 37 Yumoto, F. *et al.* Drastic Ca2+ sensitization of myofilament associated with a small structural change in
711 troponin I in inherited restrictive cardiomyopathy. *Biochemical and biophysical research communications*
712 **338**, 1519–1526 (2005). https://doi.org/10.1016/j.bbrc.2005.10.116
713 38 Klarenbeek, J., Goedhart, J., van Batenburg, A., Groenewald, D. & Jalink, K. Fourth-generation epac-based
714 FRET sensors for cAMP feature exceptional brightness, photostability and dynamic range:
715 characterization of dedicated sensors for FLIM, for ratiometry and with high affinity. *PloS one* **10**,
716 e0122513 (2015). https://doi.org/10.1371/journal.pone.0122513
717 39 Layland, J. *et al.* Essential role of troponin I in the positive inotropic response to isoprenaline in mouse
718 hearts contracting auxotonically. *J Physiol* **556**, 835–847 (2004).
719 https://doi.org/10.1113/jphysiol.2004.061176
720 40 Kentish, J. C. *et al.* Phosphorylation of troponin I by protein kinase A accelerates relaxation and
721 crossbridge cycle kinetics in mouse ventricular muscle. *Circ Res* **88**, 1059–1065 (2001).
722 https://doi.org/10.1161/hh1001.091640
723 41 Herron, T. J., Korte, F. S. & McDonald, K. S. Power output is increased after phosphorylation of
724 myofibrillar proteins in rat skinned cardiac myocytes. *Circ Res* **89**, 1184–1190 (2001).
725 https://doi.org/10.1161/hh2401.101908
726 42 Fentzke, R. C. *et al.* Impaired cardiomyocyte relaxation and diastolic function in transgenic mice
727 expressing slow skeletal troponin I in the heart. *J Physiol* **517 (Pt 1)**, 143–157 (1999).
728 https://doi.org/10.1111/j.1469-7793.1999.0143z.x
729 43 Barbato, J. C., Huang, Q. Q., Hossain, M. M., Bond, M. & Jin, J. P. Proteolytic N-terminal truncation of
730 cardiac troponin I enhances ventricular diastolic function. *J Biol Chem* **280**, 6602–6609 (2005).
731 https://doi.org/10.1074/jbc.M408525200
732 44 Venkataraman, R. *et al.* Myofilament calcium de-sensitization and contractile uncoupling prevent pause-
733 triggered ventricular tachycardia in mouse hearts with chronic myocardial infarction. *Journal of*
734 *molecular and cellular cardiology* **60**, 8–15 (2013). https://doi.org/10.1016/j.yjmcc.2013.03.022
735 45 de Waard, M. C. *et al.* Early exercise training normalizes myofilament function and attenuates left
736 ventricular pump dysfunction in mice with a large myocardial infarction. *Circ Res* **100**, 1079–1088 (2007).
737 https://doi.org/10.1161/01.RES.0000262655.16373.37
738 46 van der Velden, J. *et al.* Alterations in myofilament function contribute to left ventricular dysfunction in
739 pigs early after myocardial infarction. *Circ Res* **95**, e85–95 (2004).
740 https://doi.org/10.1161/01.RES.0000149531.02904.09
741 47 McConnell, B. K., Moravec, C. S., Morano, I. & Bond, M. Troponin I phosphorylation in spontaneously
742 hypertensive rat heart: effect of beta-adrenergic stimulation. *Am J Physiol* **273**, H1440–1451 (1997).
743 https://doi.org/10.1152/ajpheart.1997.273.3.H1440
744 48 Wolff, M. R., Buck, S. H., Stoker, S. W., Greaser, M. L. & Mentzer, R. M. Myofibrillar calcium sensitivity of
745 isometric tension is increased in human dilated cardiomyopathies: role of altered beta-adrenergically
746 mediated protein phosphorylation. *J Clin Invest* **98**, 167–176 (1996). https://doi.org/10.1172/JCI118762
747 49 Bodor, G. S. *et al.* Troponin I phosphorylation in the normal and failing adult human heart. *Circulation* **96**,
748 1495–1500 (1997). https://doi.org/10.1161/01.cir.96.5.1495
749 50 Zakhary, D. R., Moravec, C. S., Stewart, R. W. & Bond, M. Protein kinase A (PKA)-dependent troponin-I
750 phosphorylation and PKA regulatory subunits are decreased in human dilated cardiomyopathy.
751 *Circulation* **99**, 505–510 (1999).
752 51 van der Velden, J. *et al.* Increased Ca2+-sensitivity of the contractile apparatus in end-stage human heart
753 failure results from altered phosphorylation of contractile proteins. *Cardiovasc Res* **57**, 37–47 (2003).
754 https://doi.org/10.1016/s0008-6363(02)00606-5
755 52 McCarty, D. M., Monahan, P. E. & Samulski, R. J. Self-complementary recombinant adeno-associated
756 virus (scAAV) vectors promote efficient transduction independently of DNA synthesis. *Gene Ther* **8**,
757 1248–1254 (2001). https://doi.org/10.1038/sj.gt.3301514

53 Tomek, J. *et al.* T-World: A highly general computational model of a human ventricular myocyte. *bioRxiv* (2025). https://doi.org/10.1101/2025.03.24.645031

54 Richter, W. *et al.* Conserved expression and functions of PDE4 in rodent and human heart. *Basic Res Cardiol* **106**, 249–262 (2011). https://doi.org/10.1007/s00395-010-0138-8

55 Nikolaev, V. O., Bunemann, M., Hein, L., Hannawacker, A. & Lohse, M. J. Novel single chain cAMP sensors for receptor-induced signal propagation. *J. Biol. Chem.* **279**, 37215–37218 (2004).

56 Darvish, M. *et al.* Heart failure: assessment of the global economic burden. *Eur Heart J* (2025). https://doi.org/10.1093/eurheartj/ehaf323

57 Authors/Task Force, M. *et al.* 2023 Focused Update of the 2021 ESC Guidelines for the diagnosis and treatment of acute and chronic heart failure: Developed by the task force for the diagnosis and treatment of acute and chronic heart failure of the European Society of Cardiology (ESC) With the special contribution of the Heart Failure Association (HFA) of the ESC. *Eur J Heart Fail* **26**, 5–17 (2024). https://doi.org/10.1002/ejhf.3024

58 Redfield, M. M. & Borlaug, B. A. Heart Failure With Preserved Ejection Fraction: A Review. *JAMA* **329**, 827–838 (2023). https://doi.org/10.1001/jama.2023.2020

59 Redfield, M. M. *et al.* Burden of systolic and diastolic ventricular dysfunction in the community: appreciating the scope of the heart failure epidemic. *JAMA* **289**, 194–202 (2003). https://doi.org/10.1001/jama.289.2.194

60 Chahal, H. *et al.* Heart failure risk prediction in the Multi-Ethnic Study of Atherosclerosis. *Heart* **101**, 58–64 (2015). https://doi.org/10.1136/heartjnl-2014-305697

61 Lam, C. S. P., Voors, A. A., de Boer, R. A., Solomon, S. D. & van Veldhuisen, D. J. Heart failure with preserved ejection fraction: from mechanisms to therapies. *Eur Heart J* **39**, 2780–2792 (2018). https://doi.org/10.1093/eurheartj/ehy301

62 Messer, A. E., Jacques, A. M. & Marston, S. B. Troponin phosphorylation and regulatory function in human heart muscle: dephosphorylation of Ser23/24 on troponin I could account for the contractile defect in end-stage heart failure. *J Mol Cell Cardiol* **42**, 247–259 (2007). https://doi.org/10.1016/j.yjmcc.2006.08.017

63 Feng, H. Z., Huang, X. & Jin, J. P. N-terminal truncated cardiac troponin I enhances Frank-Starling response by increasing myofilament sensitivity to resting tension. *J Gen Physiol* **155** (2023). https://doi.org/10.1085/jgp.202012821

64 Thompson, B. R., Martindale, J. & Metzger, J. M. Sarcomere neutralization in inherited cardiomyopathy: small-molecule proof-of-concept to correct hyper-Ca2+-sensitive myofilaments. *American journal of physiology. Heart and circulatory physiology* **311**, H36–43 (2016). https://doi.org/10.1152/ajpheart.00981.2015

65 Joyce, W. *et al.* Genetic excision of the regulatory cardiac troponin I extension in high-heart rate mammal clades. *Science* **385**, 1466–1471 (2024). https://doi.org/10.1126/science.adi8146

66 Dominic, K. L., Schmidt, A. V., Granzier, H., Campbell, K. S. & Stelzer, J. E. Mechanism-based myofilament manipulation to treat diastolic dysfunction in HFpEF. *Front Physiol* **15**, 1512550 (2024). https://doi.org/10.3389/fphys.2024.1512550

67 Landim-Vieira, M. & Pinto, J. R. Can evolution-based studies inform modern medicine? *Science* **385**, 1420–1421 (2024). https://doi.org/10.1126/science.ads2585

68 Sumandea, C. A. *et al.* Cardiac troponin T, a sarcomeric AKAP, tethers protein kinase A at the myofilaments. *The Journal of biological chemistry* **286**, 530–541 (2011). https://doi.org/10.1074/jbc.M110.148684

69 Fentzke, R. C. *et al.* Impaired cardiomyocyte relaxation and diastolic function in transgenic mice expressing slow skeletal troponin I in the heart. *J Physiol* **517 (Pt 1)**, 143–157 (1999). https://doi.org/10.1111/j.1469-7793.1999.0143z.x

70 Hamo, C. E. *et al.* Heart failure with preserved ejection fraction. *Nat Rev Dis Primers* **10**, 55 (2024). https://doi.org/10.1038/s41572-024-00540-y

Figures

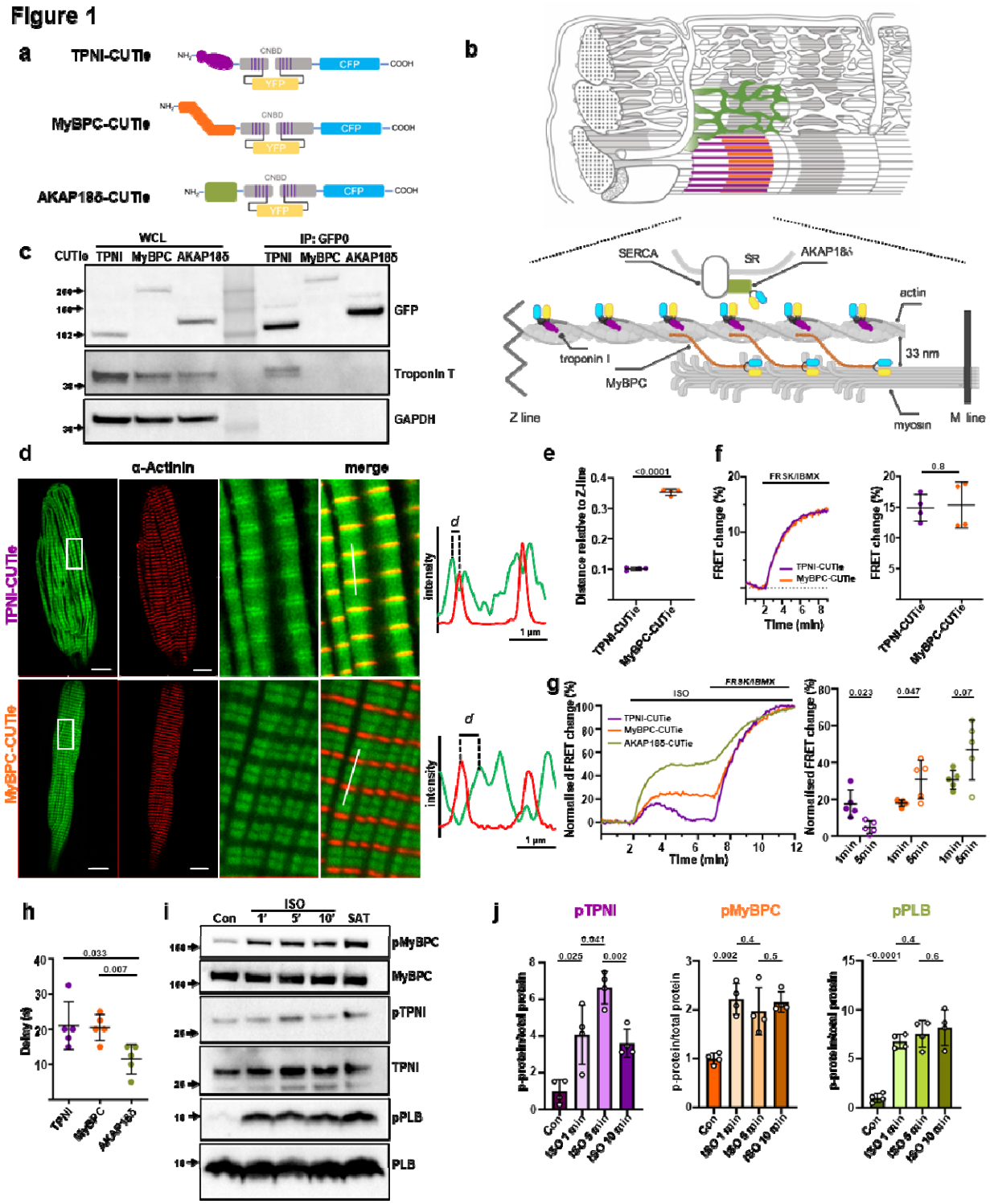
Figure 1
a
TPNI-CUTie
MyBPC-CUTie
AKAP18δ-CUTie
CNBD
CFP
YFP
COOH
b
SERCA
SR
AKAP18δ
actin
troponin I
MyBPC
33 nm
Z line
myosin
M line
c
WCL
IP: GFP0
CUTie TPNI MyBPC AKAP18δ
GFP
Troponin T
GAPDH
d
α-Actinin
merge
TPNI-CUTie
MyBPC-CUTie
intensity
1 µm
e
Distance relative to Z-line
<0.0001
f
FRSK/IBMX
FRET change (%)
Time (min)
0.8
g
ISO
Normalised FRET change (%)
AKAP18δ-CUTie
0.023
0.047
0.07
h
Delay (s)
0.033
0.007
TPNI
MyBPC
AKAP18δ
i
ISO
Con
1'
5'
10'
SAT
pMyBPC
MyBPC
pTPNI
TPNI
pPLB
PLB
j
pTPNI
pMyBPC
pPLB
p-protein/total protein
0.041
0.025
0.002
0.4
0.5
<0.0001
0.6
Con
ISO 1 min
ISO 5 min
ISO 10 min

Figure 1 - Unique cAMP regulation at TPNI. (a) Schematic representation of the FRET targeted reporters TPNI-, MyBPC- and AKAP18d-CUTie and (**b**) depiction of their subcellular localisation in the cardiac myocyte. CNBD = cAMP binding domain. (**c**) Western blot of GFP immunoprecipitation from lysates of NRVM expressing TPNI-, MyBPC- or AKAP18δ-CUTie and probed with GFP or Troponin T antibody. Representative of three independent experiments. (**d**) Representative confocal images of ARVM expressing TPNI-CUTie or MyBPC-CUTie showing sensor localisation relative to α-actinin. A magnified detail and a merged image of the sensor (green) and α-actinin localisation (red) are also shown. For each sensor, fluorescence intensity profiles measured across a single sarcomere along the line indicated in the zoomed-in merged images are presented in the panels on the right. Dotted lines indicate peak intensity for the α-actinin and sensor signal used to determine the distance (*d*) between the sensor localisation and the Z line, quantified in (**e**). Groups compared by two-tailed unpaired t-test with Welch's correction. (**f**) Representative kinetics and average of maximal FRET change displayed by the TPNI- or MyBPC-CUTie sensors expressed in HEK293 cells in response to a saturating stimulus (25 μM FRSK + 100 μM IBMX). Two-tailed unpaired t-test with Welch's correction. (**g**) Representative kinetics (left) and quantification of FRET change at 1 min and 5 min after application of 5 nM ISO (right) recorded in ARVM expressing the targeted CUTie reporters. Forskolin (FRSK, 25 μM) and IBMX, (100 μM) were applied at the end of the experiment to achieve sensor saturation. Two-tailed paired t-test. (**h**) Average time to achieve 5% of FRET change after 5 nM ISO application. Two-tailed unpaired t-test with Welch's correction. (**i**) Representative western blot of ARVM lysates showing total protein amount and phosphorylation level at 1 min, 5 min and 10 min after application of 5 nM ISO for MyBPC, TPNI and PLB. (**j**) Quantification of experiments as in (i). Two-tailed unpaired t-test with Welch's correction.

For all experiments, data points represent an independent experiment, $n \geq 4$ biological replicates. All Values are means ± SD.

Figure 2

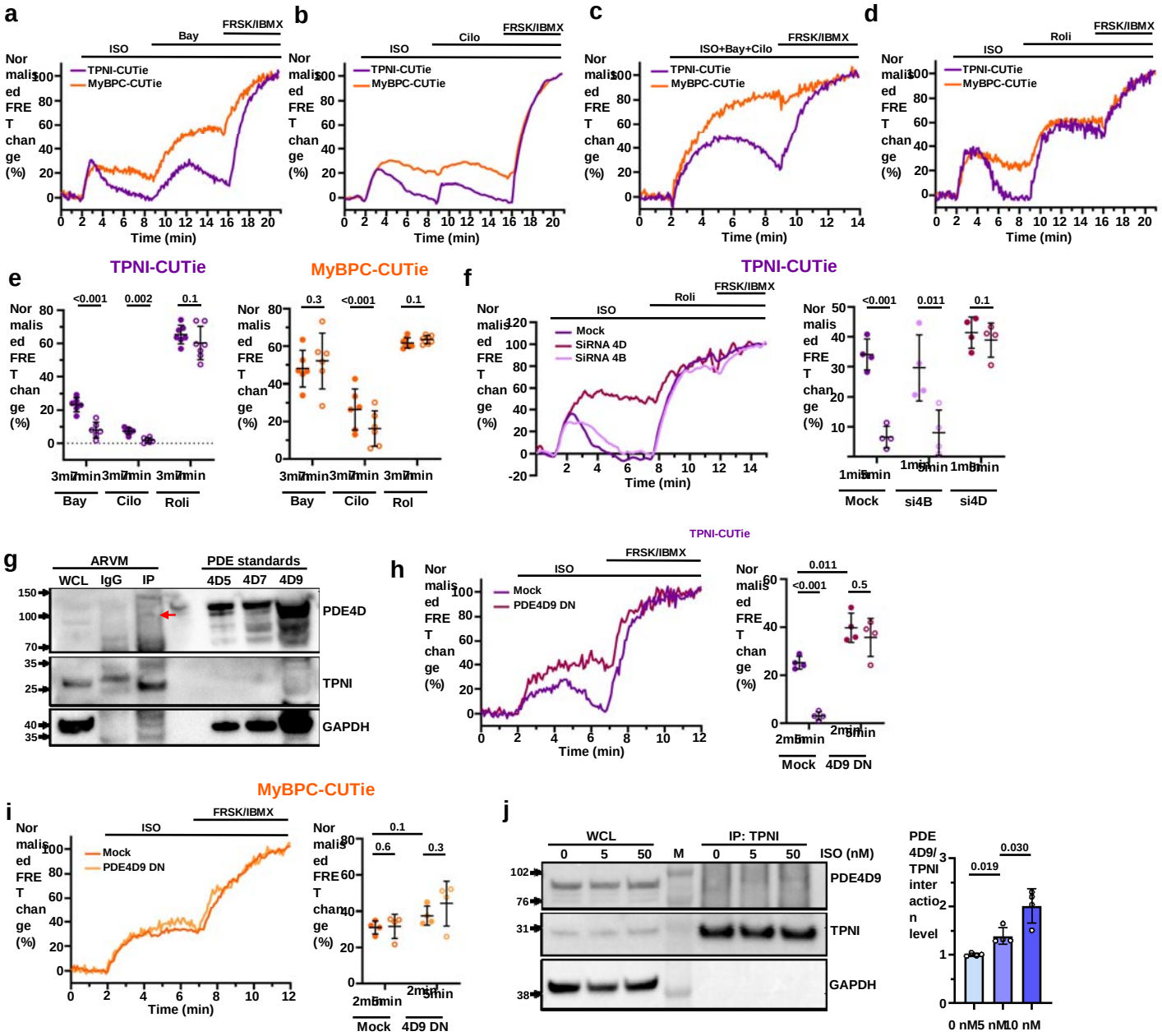

Figure 2 - PDE4D9 regulates cAMP at TPNI. Representative kinetics of FRET change recorded in NRVM expressing TPNI- or MyBPC-CUTie and treated with 1nM ISO followed by either (**a**) BAY, (10 nM), (**b**) Cilostamide, (10 μM), (**c**) BAY (10 nM) + Cilostamide (10 μM), or (**d**) Rolipram (10 μM). (**e**) Summary of

cAMP responses measured at 3 min and 7 min after inhibitor application in experiments as shown in (a), (b) and (d). Two-ailed paired t-test. (**f**) Representative kinetics and summary of FRET change recorded at 1 min and 5 min after the application of 1nM ISO in NRVM expressing TPNI-CUTie and where PDE4D or PDE4B were knockdown by siRNA. Cells were subsequently treated with Rolipram (10 μM) and saturating treatment (FRSK 25 μM + IBMX 100 μM). Two-tailed paired t-test. (**g**) Representative Western blot of TPNI immunoprecipitate (IP) probed with a pan PDE4D antibody. Lysates obtained from CHO cells overexpressing PDE4D5, PDE4D7 and PDE4D9 (PDE standards) are shown as a reference for molecular weight. (**h**) Representative kinetics and summary of FRET change recorded at 2 min and 5 min after application of 1nM ISO in NRVM expressing PDE4D9-mCherry dominant negative (PDE4D9 DN) construct and either TPNI-CUTie or (**i**) MyBPC-CUTie. Two-tailed paired and unpaired t-test. (**j**) Representative Western blot and quantification of whole cell lysate (WCL) and TPNI immunoprecipitate generated from NRVM treated with different concentrations of ISO, as indicated and detection of PDE4D9 using a PDE4D9-specific antibody. Two-tailed unpaired t-test with Welch's correction.

Each data point represents an independent experiment, $n \geq 4$ biological replicates. All values are means ± SD.

Figure 3

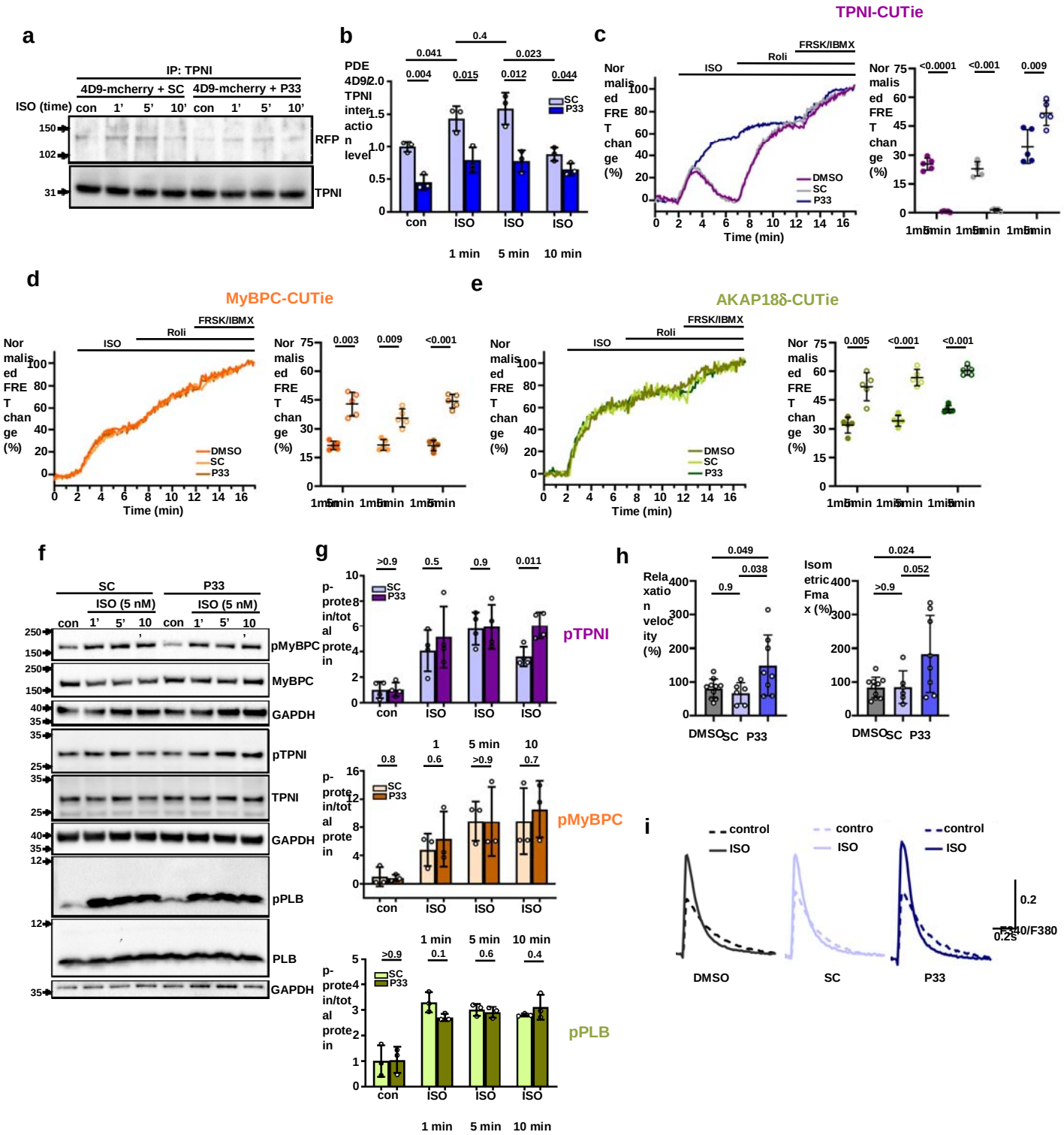

Figure 3 - P33 selectively enhances cAMP at TPNI and improves cardiac contractility *in vitro*. (**a**) Representative Western blot and (**b**) quantification of co-immunoprecipitation from NRVM overexpressing

PDE4D9-mCherry treated with ISO (1 nM) and P33 peptide (10 μM) or control SC peptide (10 μM). Two-tailed unpaired t-test with Welch's correction. Representative kinetics and summary of FRET change recorded at 1 min and 5 min in NRVM overexpressing (**c**) TPNI-CUTie, (**d**) MyBPC-CUTie or (**e**) AKAP18δ-CUTie and treated with 1 nM ISO. Cells were pre-treated with DMSO, SC (10 μM) or P33 (10 μM), as indicated. Two-tailed paired t-test. (**f**) Representative Western blot and (**g**) quantification showing total protein and phosphorylation time course for TPNI and MyBPC in ARVM pre-treated with 10 μM P33 peptide or control SC peptide and lysed 1 min, 5 min or 10 min after application of 5 nM ISO. Two-tailed unpaired t-test with Welch's correction. (**h**) Maximal isometric force response and relaxation velocity measured in isolated ARVM. One-way ANOVA with Tukey post-hoc correction. Each data point represents an independent experiment, $n \geq 3$ biological replicates. All values are means ± SD. (**i**) Average Calcium transients recorded in ARVM under unstimulated conditions (control) or in response to 5 nM ISO. Cells were pre-treated with DMSO, SC (10 μM), or P33 (10 μM), as indicated. Exemplary average curves are obtained from paced transients (at least 10 transients) from one cell, normalised to fluorescence ratio at time point 0s. Representative of $n \geq 4$ biological replicates.

Figure 4

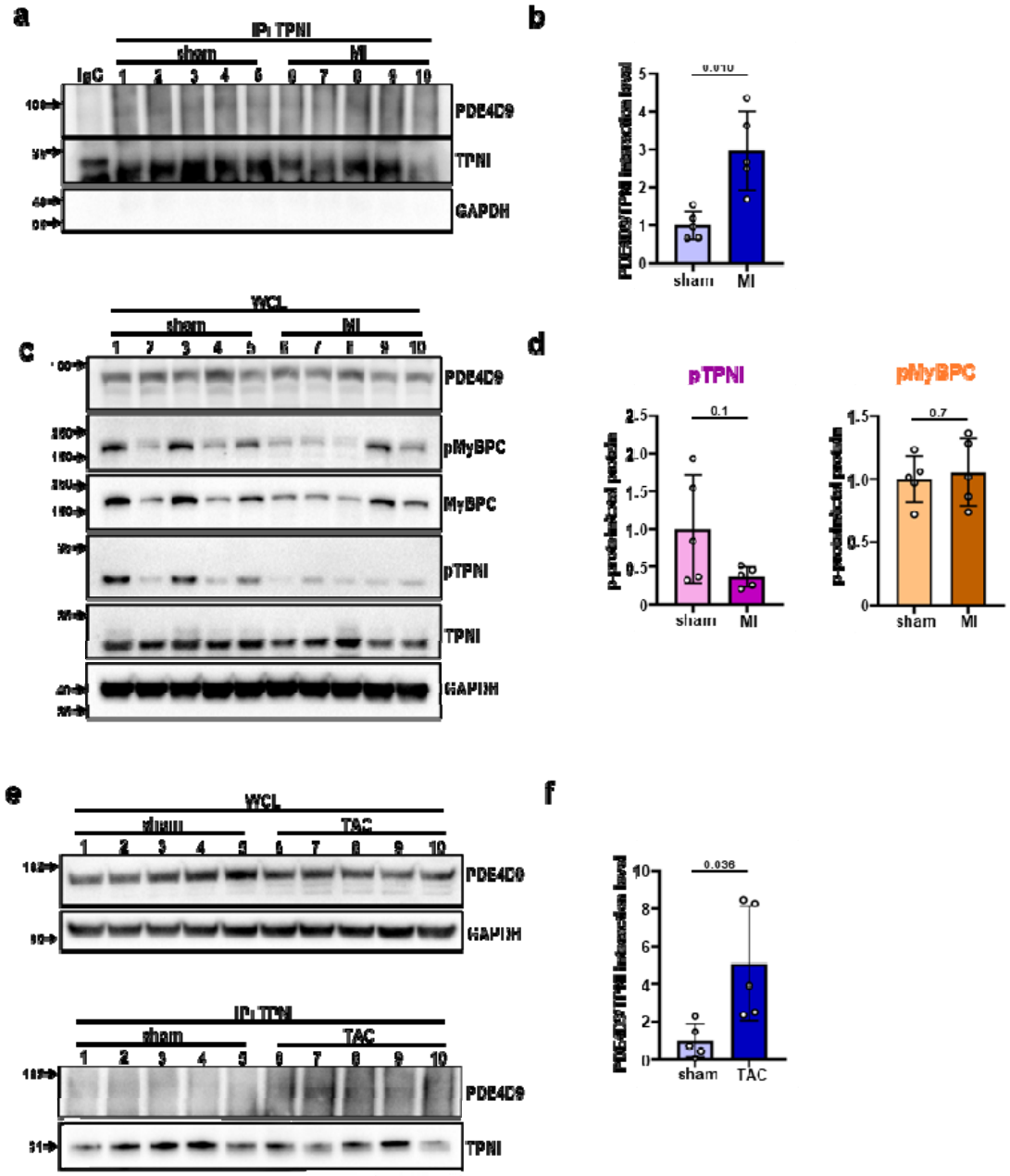

Figure 4 - Interaction of PDE4D9 with TPNI is enhanced in cardiac disease. (**a**) Representative co-immunoprecipitation and (**b**) quantification of PDE4D9/TPNI interaction using lysates from mouse heart tissue obtained from sham or myocardial infarcted (MI) hearts. (**c**) Representative western blot and (**d**) quantification of TPNI and MyBPC phosphorylation in whole cell lysates (WCL) from sham or myocardial infarcted (MI) mouse

hearts. (**e**) Representative co-immunoprecipitation and (**f**) quantification of PDE4D9/TPNI interaction in protein lysates isolated from sham or transverse aortic banding (TAC) mouse hearts. Two-tailed unpaired t-test with Welch's correction. Lane numbers indicate individual animals. n = 5 for each group. All values are means ± SD.

Figure 5

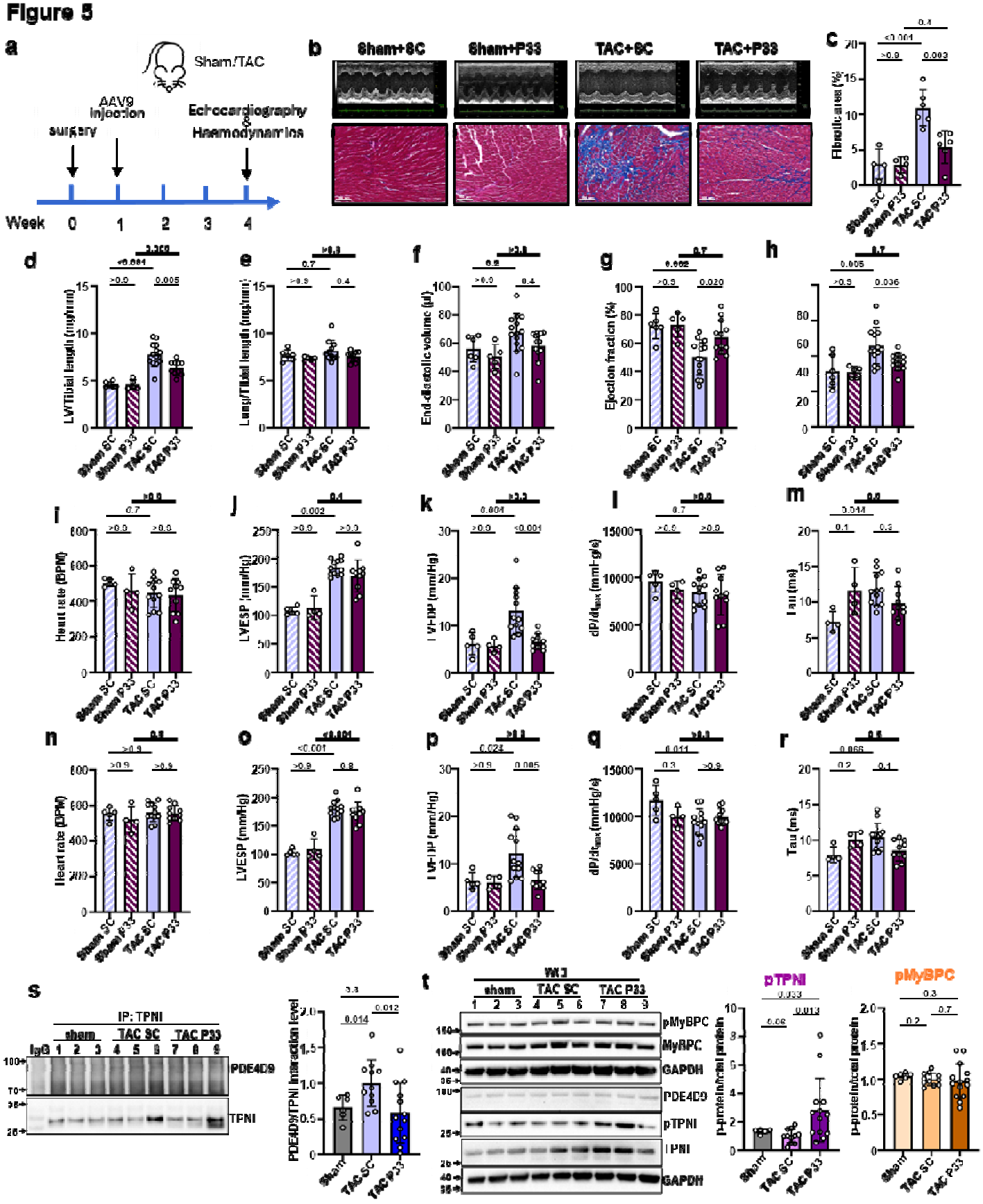
a
Sham/TAC
AAV9 injection
surgery
Echocardiography & Haemodynamics
Week 0 1 2 3 4
b
Sham+SC
Sham+P33
TAC+SC
TAC+P33
c
Fibrotic area (%)
d
LV/Tibial length (mg/mm)
e
Lung/Tibial length (mg/mm)
f
End-diastolic volume (µl)
g
Ejection fraction (%)
h
i
Heart rate (BPM)
j
LVESP (mmHg)
k
LVEDP (mmHg)
l
dP/dt max (mmHg/s)
m
Tau (ms)
n
Heart rate (BPM)
o
LVESP (mmHg)
p
LVEDP (mmHg)
q
dP/dt max (mmHg/s)
r
Tau (ms)
Sham SC
Sham P33
TAC SC
TAC P33
s
IP: TPNI
sham
TAC SC
TAC P33
IgG 1 2 3 4 5 6 7 8 9
PDE4D9
TPNI
PDE4D9/TPNI interaction level
t
WB
sham
TAC SC
TAC P33
1 2 3 4 5 6 7 8 9
pMyBPC
MyBPC
GAPDH
PDE4D9
pTPNI
TPNI
GAPDH
pTPNI
p-protein/total protein
pMyBPC
p-protein/total protein
Sham
TAC SC
TAC P33

888

Figure 5 - P33 protects from pressure overload-induced cardiac dysfunction. (**a**) Treatment protocol: wild-type mice were treated with scAAV9-SC or scAAV9-P33 via tail vein injection one week after sham or transverse aortic banding (TAC) surgery. Organ weights, echocardiographic parameters and left ventricular (LV) haemodynamics were obtained three weeks post-injection. (**b**) Representative M-mode echocardiography scans (top) and Masson's trichrome staining at week 4 after TAC (bottom; scale bar = 100 μm). (**c**) Quantification of the normalized fibrotic area (%). Sham-SC n = 4, sham-P33 n =4, TAC+SC n = 6 and TAC+P33 n = 6. (**d**) Left ventricle and (**e**) lung weights obtained post-mortem and normalised to tibial length. (**f**) Echocardiography showing LV end diastolic volume, (**g**) LV ejection fraction and (**h**) the diastolic parameter E/e' derived from combining Pulse-wave Doppler and Tissue Doppler imaging. Haemodynamics measured under (**i-m**) basal and (**n-r**) cardiac stressor dobutamine (32 ng/g BW/min) for heart rates, left ventricular end-systolic pressure (LVESP), left ventricular end-diastolic pressure (LVEDP), the maximum rate of pressure rise (dP/dt_{max}) as a measure of contractility, isovolumetric constant, tau, as a measure of relaxation. Sham-SC N≥ 5, Sham-P33 N ≥ 4, TAC-SC ≥ 12, TAC-P33 ≥ 10. Ordinary one-way ANOVA with Sidak post-hoc correction, Kruskal-Wallis with Dunn's correction was used when values failed the normality test. All values are mean ± SD. (**s**) Representative western blot and quantification of PDE4D9/TPNI interaction in cardiac tissue collected 4 weeks after surgery from sham operated or TAC operated mice and treated either with SC or P33. (**t**) Representative western blot and quantification of TPNI phosphorylation level in the same samples as in (s). Groups were compared by two-tailed unpaired t-test with Welch's correction. Lane numbers and data point represent an individual animal. n ≥ 6 for each group. All values are means ± SD.

913

Figure 6

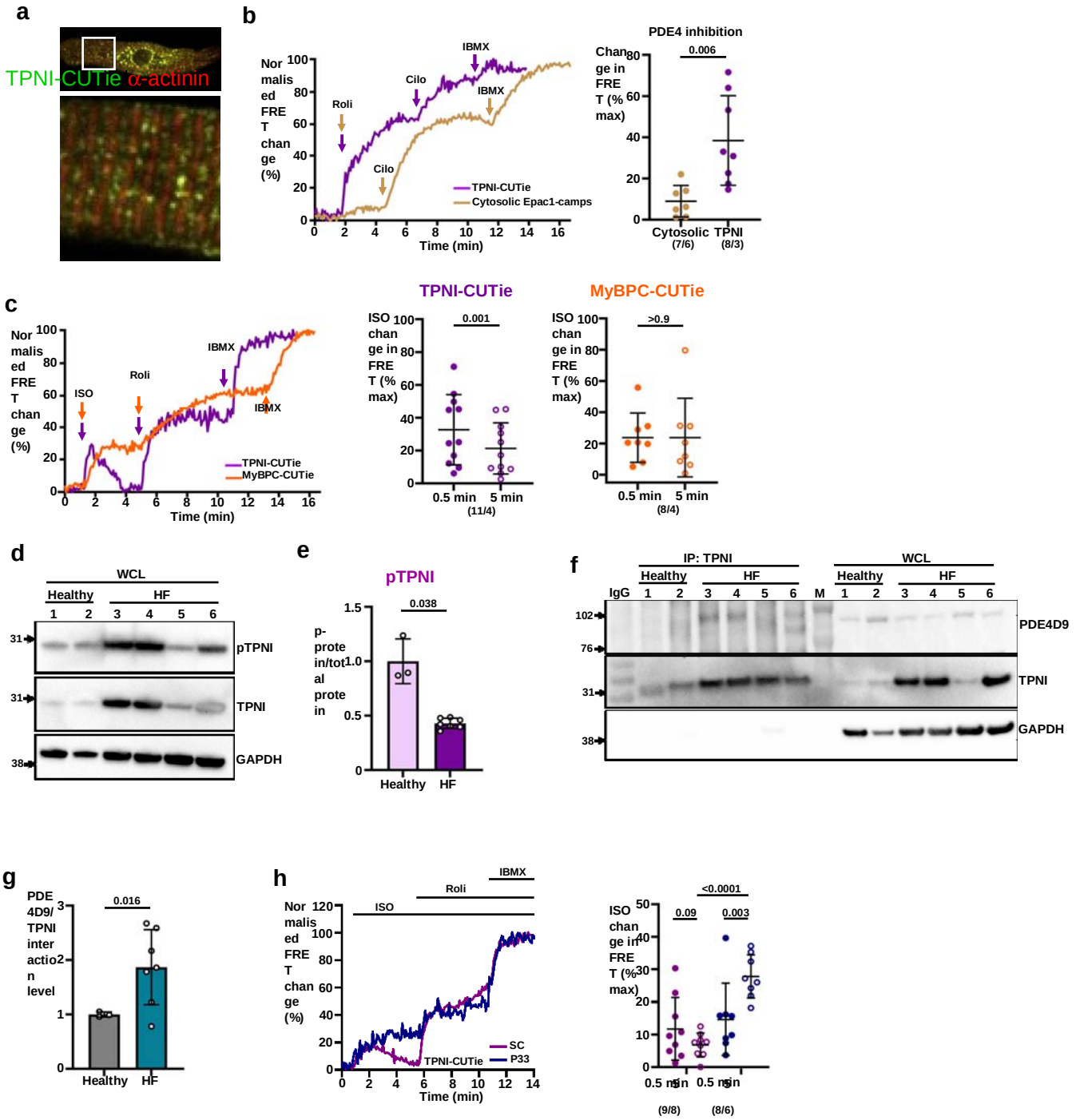

914

Figure 6 - Role of PDE4D and modulation by P33 in human cardiac myocytes. (**a**) Representative image of human ventricular myocyte expressing TPNI-CUTie (green) and stained with α-actinin-specific antibody (red) **(b)** Representative kinetics and summary of FRET change in response to PDE4 inhibitor Rolipram (Roli, 10 μM) recorded in human ventricular myocytes isolated from patients with heart failure with reduced ejection fraction (HFrEF) and expressing TPNI-CUTie or the cytosolic Epac1-camps sensor. The kinetics also show the response to PDE3 inhibition with Cilostamide, (10 μM) and IBMX (100 μM). Each compound was added to the bath in sequence without washout between additions. Arrows indicate the time of compound addition. Two-tailed unpaired t-test with Welch's correction. **(c)** Representative kinetics and summary of the FRET change at 0.5 min and 5 min after the application of ISO (1 nM) recorded in human ventricular myocyte isolated from HFrEF patients and expressing TPNI-CUTie or MyBPC-CUTie targeted sensors. The effect of applying Rolipram (10 μM) and IBMX (100 μM) is also shown. Two-tailed paired t-test. Each data point represents an independent experiment. Cells are from 4 different individuals**. (d)** Representative western blot and **(e)** summary of TPNI phosphorylation levels in lysates from healthy human donors and patients with reduced EF. Two-tailed unpaired t-test with Welch's correction. **(f)** Representative western blot and **(g)** summary of TPNI immunoprecipitation probed with PDE4D9 antibody using the same samples as in (d). Two tailed unpaired t-test with Welch's correction. Each data point represents an individual patient. Healthy donor n = 3, HF patients n = 7. **(h)** Representative kinetics and summary of FRET change at 0.5 min and 5 min after application of ISO (5 nM) recorded in human ventricular myocytes isolated from HFrEF patients, pre-treated with SC or P33 peptides and expressing the TPNI-CUTie targeted sensor. A typical response to Rolipram (10 μM) and IBMX (100 μM) application is also shown. Two tailed paired t-test for comparisons between 0.5 min and 5 min. Two-tailed unpaired t-test with Welch's corrections for comparison between SC and P33 at 5 min. Each data point represents an independent experiment. For both treatments, data are from six different patients. Number of cells is also indicated under the graphs. All values are means ± SD.